Electronic Supplementary Material (ESI) for Catalysis Science & Technology.

Supplementary Information

Density functional theory and microkinetics of ethylene chain growth and termination on silica grafted group 4 metal hydrides

Neha Mehra and William F. Schneider*

Department of Chemical and Biomolecular Engineering, University of Notre Dame, Notre Dame, Indiana 46556, United States

*E-mail: wschneider@nd.edu

Table of Contents

Multi-product reaction cycle and assumptions

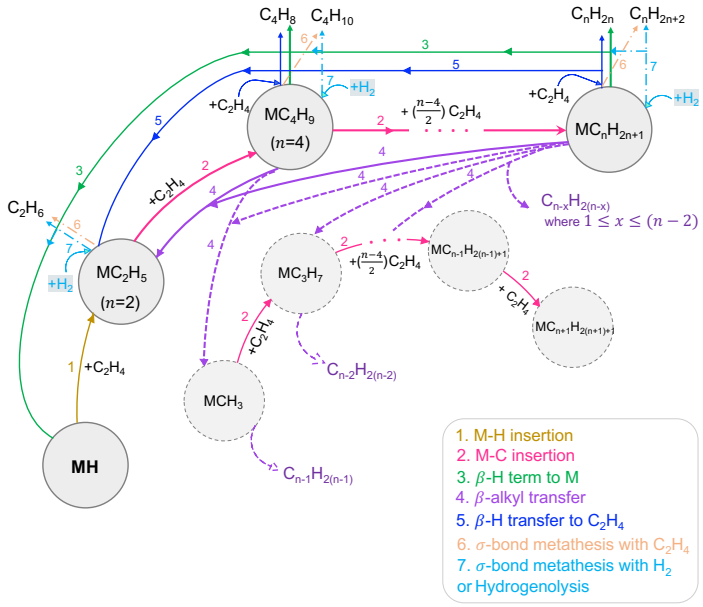

Formula	n	Structure	$1 \le x \le (n-2)$	MC_xH_{2x+1}	$C_{n-x}H_{2(n-x)}$
MC_4H_9	4		2	MC_2H_5	C_2H_4
	4		1	MCH_3	C_3H_6
	4		1	MCH_3	C_3H_6

When $\mathbf{1 \le x \le (n-2)}$; β-alkyl transfer to M
$\boldsymbol{x}$ = 0 ; β-H transfer to M

Scheme S1: Schematic summary of reactions relevant to ethylene (C_2H_4) oligomerization on MH (M=metal ion) sites, color coded by reaction type. Surface sites are enclosed in bubbles. Solid circular bubble on bottom left: insertion of ethylene into M-H (1) forms MC_2H_5 that proceeds to form linear chained MC_4H_9 by ethylene insertion into M-C bond (2), leading to chain growth by C-C bond formation. β-H elimination to M (3) or to an ethylene monomer (5), or β-alkyl transfer to metal (4), all lead to olefin. σ-bond metathesis with ethylene (6) or with H_2 (7) yields saturated products and either generates M-vinyl that can undergo ethylene insertion to form alkylidene chains (not shown here) or restores the M-H site.

Secondary reactions of olefins begin by reinsertion at an internal olefinic carbon. Repeated termination-insertion steps result in chain-walking, and through β-alkyl transfer (table shows possibilities for MC_4H_9), to odd-numbered C chains or their surface sites (dashed bubbles).

Microkinetic models assume that rate constants for the 7 distinct reaction types are independent of the chain length. Further, we neglect the contributions of reinsertion reactions, thus assuming that transport from active sites is more rapid than reinsertion reactions.

Raw gas molecule energies

Table S1: PBE computed (E^{DFT}) and zero-point (E^{ZPE}) energies in eV for gas molecules enclosed in 15Å x 15Å x 15Å cell

	E^{DFT}	E^{ZPE}
Ethene (C_2H_4)	-31.971	1.359
1-Butene (1-C_4H_8)	-65.179	2.884
Ethane (C_2H_6)	-40.494	1.989
Methane (CH_4)	-24.031	1.188
Hydrogen (H_2)	-6.760	0.272
Water (H_2O)	-14.222	0.573
$Si(OH)_4$	-52.020	1.531
$Ti(CH_3)_4$	-86.542	3.605
$Zr(CH_3)_4$	-87.462	3.584
$Hf(CH_3)_4$	-89.322	3.592

Silica surfaces representations

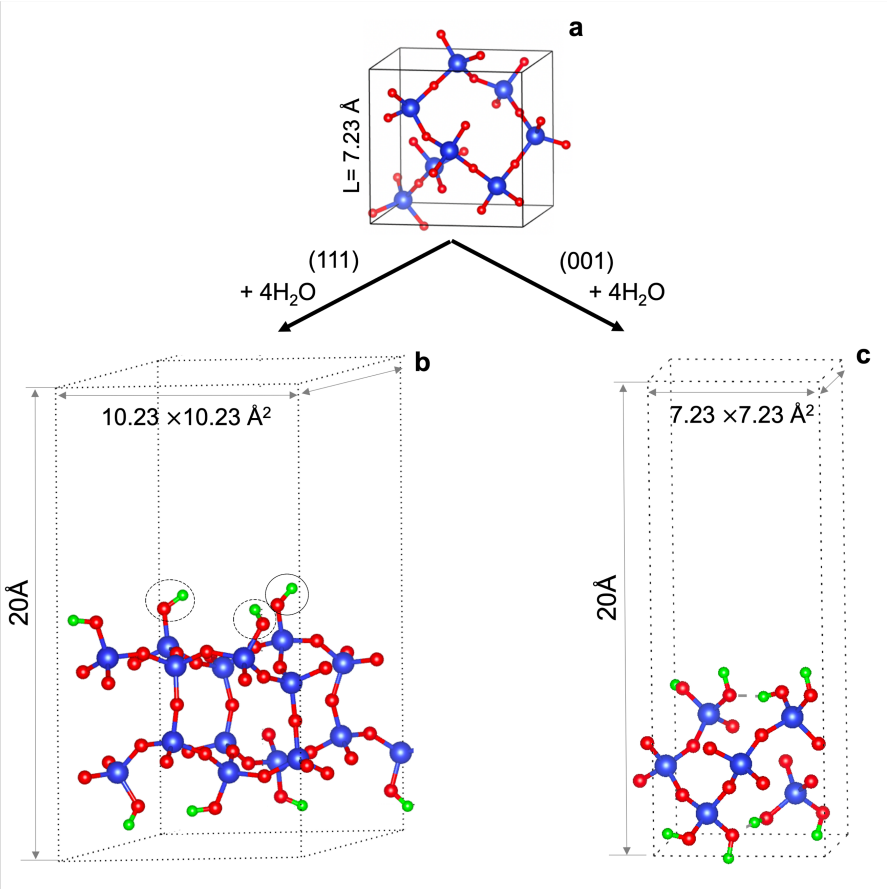

Fig. S1: a) Bulk β-cristobalite[1] unit cell **b)** (111) silica surface having 4 OH groups on top surface **c)** (001) silica surface with geminal silanols (two OH groups on a Si). Atoms are colored as H in green (●), O in red (●), Si in blue (●).

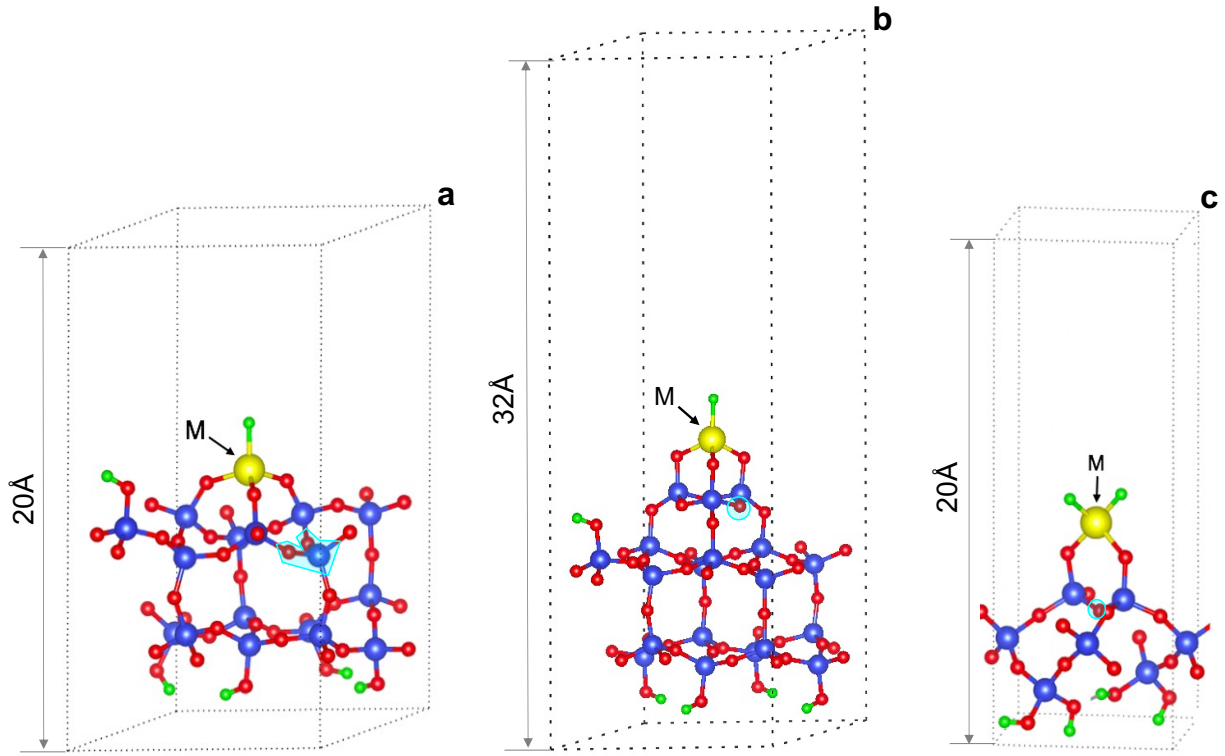

Fig. S2: a) 3-4mr $(\equiv SiO)_3MH$ on (111) silica **b)** 3-3mr $(\equiv SiO)_3MH$ on reconstructed (111) silica **c)** 1-3mr $(\equiv SiO)_2MH_2$ on dehydroxylated (001) surface. Linkages separating the M-O-Si bonds are marked in light blue shade.

Grafting and hydrogenolysis of $M(CH_3)_4$ to 3-4mr site

Grafting is performed with the precursor $M(CH_3)_4$ on silanols of silica surface. The sequential reactions leading to formation of M(IV) hydrides are presented in reaction (s1) and reaction (s2) where n=1,2 or 3 for silica (111). The goal is to compare the relative stabilities of these species and not to reproduce the actual grafting process where breaking of strained siloxane (≡Si-O-Si≡) bridges and generation of silicon hydrides $Si\text{-}H_x$ accompany the formation of M(IV)-hydrides.

$$n(\equiv Si\text{-}OH) + (CH_3)_4M \rightarrow (\equiv SiO)_nM(CH_3)_{4-n} + nCH_4 \quad (s1)$$

$$(\equiv SiO)_nM(CH_3)_{4-n} + (4-n)H_2 \rightarrow (\equiv SiO)_nM(H)_{4-n} + (4-n)CH_4 \quad (s2)$$

Structures of $(\equiv SiO)_nM(CH_3)_{4-n}$, obtained from reaction (s1) are in Fig. S3 and their energies in Table S2. Thermodynamics associated with the sequential loss of methyl ligand as the metal ion anchors to single silanols of silica (111) is shown for Zr^{4+} ion in Fig. S4(a). A parity plot comparing heats of grafting (listed in Table S3) for $(\equiv SiO)_nM(CH_3)_{4-n}$ complexes over (111) surface for the three metal ions against Zr's is shown in Fig. S4(b). The heats of grafting are in the order of Hf < Zr < Ti and are exothermic. This is in line with M-O and M-C bond energies reported in literature[2] (Table S4).

Hydrogenolysis of $(\equiv SiO)_nZr(CH_3)_{4-n}$ complexes to their corresponding hydrides $(\equiv SiO)_nZr(H)_{4-n}$ (structures in Fig. S5) as per reaction (s2) is exothermic (Table S3). Hydrogenolysis energy varies non-periodically across metal ions as Ti > Zr < Hf. The H-bonding between the M-hydride and H^+ of ≡SiOH in the vicinity, enhances the stability of $(\equiv SiO)M(H)_3$ and $(\equiv SiO)_2M(H)_2$, while such an interaction is not there in $(\equiv SiO)_3M(H)$ (Fig. S5). Overall, this indicates that supported organic complexes of Group-4 metals when pre-treated with hydrogen will convert to hydrides that have higher coordination to support as reported by experimental characterizations.

Table S2: PBE computed $\boldsymbol{E^{DFT}}$ **(***without ZPE correction*) energies in eV for structures in grafting and hydrogenolysis reactions on (111) silica of Fig. S1b

Species	**Ti**	**Zr**	**Hf**
$(\equiv SiO)M(CH_3)_3$	-501.691	-502.706	-504.678
$(\equiv SiO)_2M(CH_3)_2$	-479.322	-480.612	-482.615
$(\equiv SiO)_3M(CH_3)$	-456.819	-458.182	-460.223
$(\equiv SiO)M(H)_3$	-450.350	-451.514	-453.406
$(\equiv SiO)_2M(H)_2$	-445.390	-446.626	-448.612
$(\equiv SiO)_3M(H)$	-439.705	-441.116	-443.153
Clean Silica slab	-437.004		

Table S3: DFT computed heats of grafting $(CH_3)_4M$ in eV on silica (111) surface using energies from Table S2

M	**Grafting $M(CH_3)_4$ on silica (111)**			**Hydrogenolysis of grafted $(\equiv SiO)_nM(CH_3)_{4-n}$**		
	Calculated by reaction (s1)			**Calculated by reaction (s2)**		
	n=1	**n=2**	**n=3**	**n=1**	**n=2**	**n=3**
Ti	-2.18	-3.84	-5.37	-0.47	-0.61	-0.16
Zr	-2.27	-4.21	-5.81	-0.62	-0.56	-0.21
Hf	-2.38	-4.35	-5.99	-0.54	-0.54	-0.20

Table S4: M-C and M-O bond energy trends for Ti, Zr and Hf compounds from literature.[2] Energies in kcal/mol

Bond	**Compounds from reference**	**Bond Energies[2]**	**Average Energy of M-O, M-C bonds**	**|(M-O)-(M-C)|**
Ti-C	$Ti(CH_2CMe_3)_4$	44	57	**55**
	$Ti(CH_2SiMe_3)_4$	64		
	$Ti(CH_2Ph)_4$	63		
Ti-O	$Ti(OPr^i)_4$	112	112	
Zr-C	$Zr(CH_2CMe_3)_4$	54	68	**68**
	$Zr(CH_2SiMe_3)_4$	75		
	$Zr(CH_2Ph)_4$	74		
Zr-O	$Zr(OPr^i)_4$	136	136	
Hf-C	$Hf(CH_2CMe_3)_4$	58	58	**79**
Hf-O	$Hf(OPr^i)_4$	137	137	

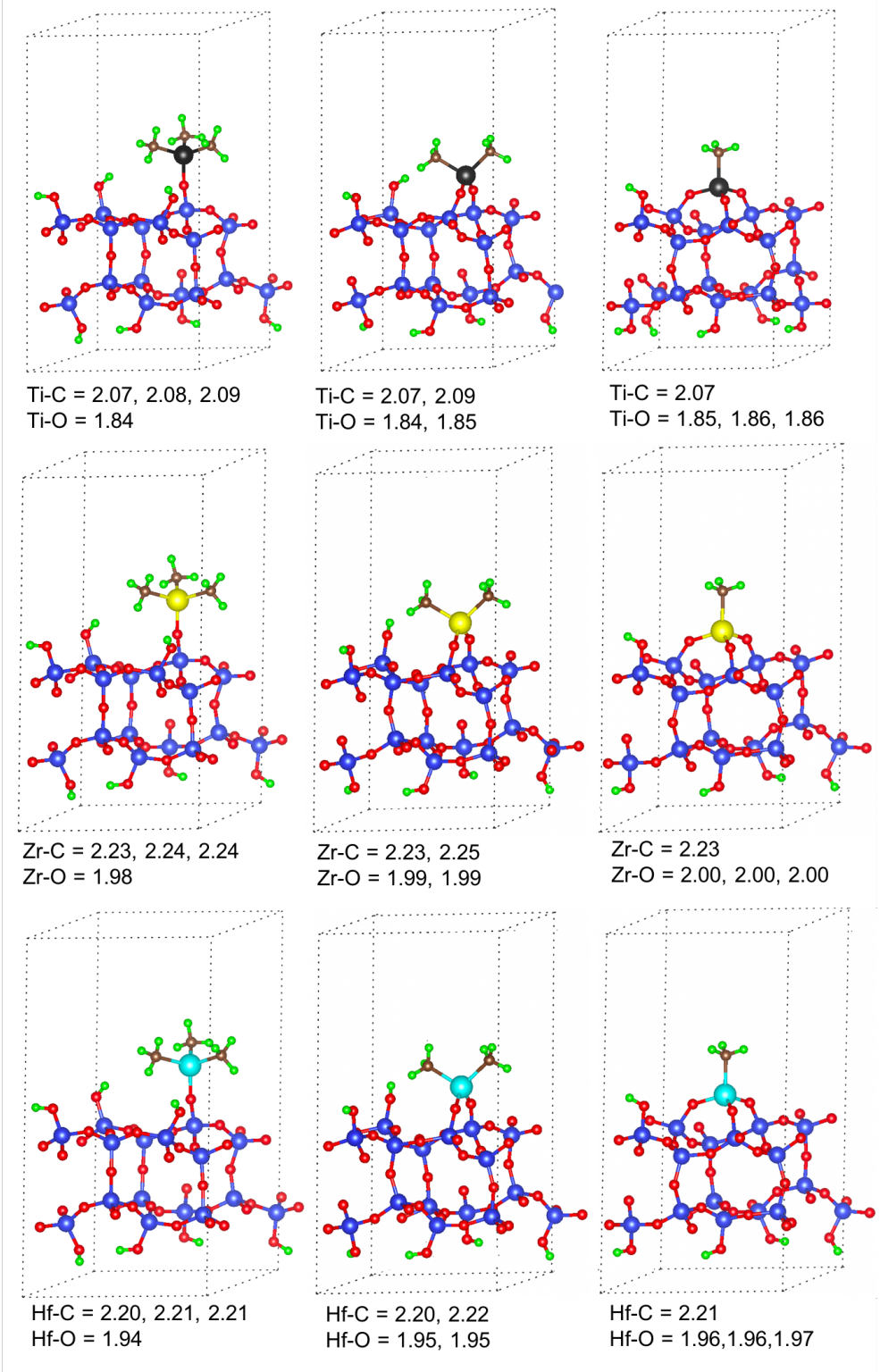

Fig. S3: Structures of $(\equiv SiO)_nM(CH_3)_{4-n}$ on silica(111). Top row for M= Ti, second row for M= Zr, and third row for M= Hf with n = 1, 2, 3 (from left to right). Atoms are colored as H: green, C: brown, O: red, Si: blue, Ti: black (●), Zr: yellow (●), Hf: cyan (light blue, ●). All distances in Å. CONTCARs in Zenodo.[11]

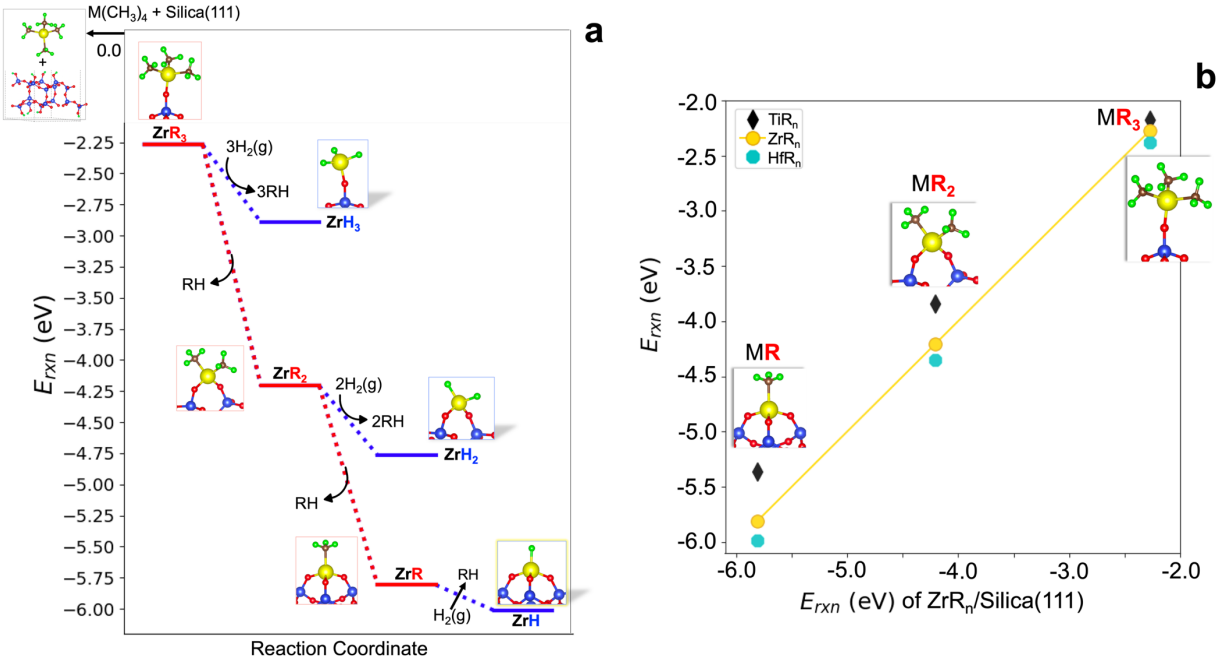

Fig. S4 a) Heats of formation of $(\equiv SiO)_nZr(CH_3)_{4-n}$ (R= CH_3) and $(\equiv SiO)_nZr(H)_{4-n}$ on silica (111) [n= 1,2,3] **b)** Parity plot comparing heats of formation of $(\equiv SiO)_nM(CH_3)_{4-n}$ for Ti, Zr and Hf on silica (111) against $(\equiv SiO)_nZr(CH_3)_{4-n}$.

Table S5: Comparison of wavenumbers (cm^{-1}) of M-H bond stretching for 3-4mr monohydride, $(\equiv SiO)_3M(H)$ sites to the experimentally reported values

	TiH	**ZrH**	**HfH**
DFT	1756	1689	1725
Experimental	1706, 1692, 1679, and 1647,[9] 1600-1725[3]	1633[4,5]	1701[6]

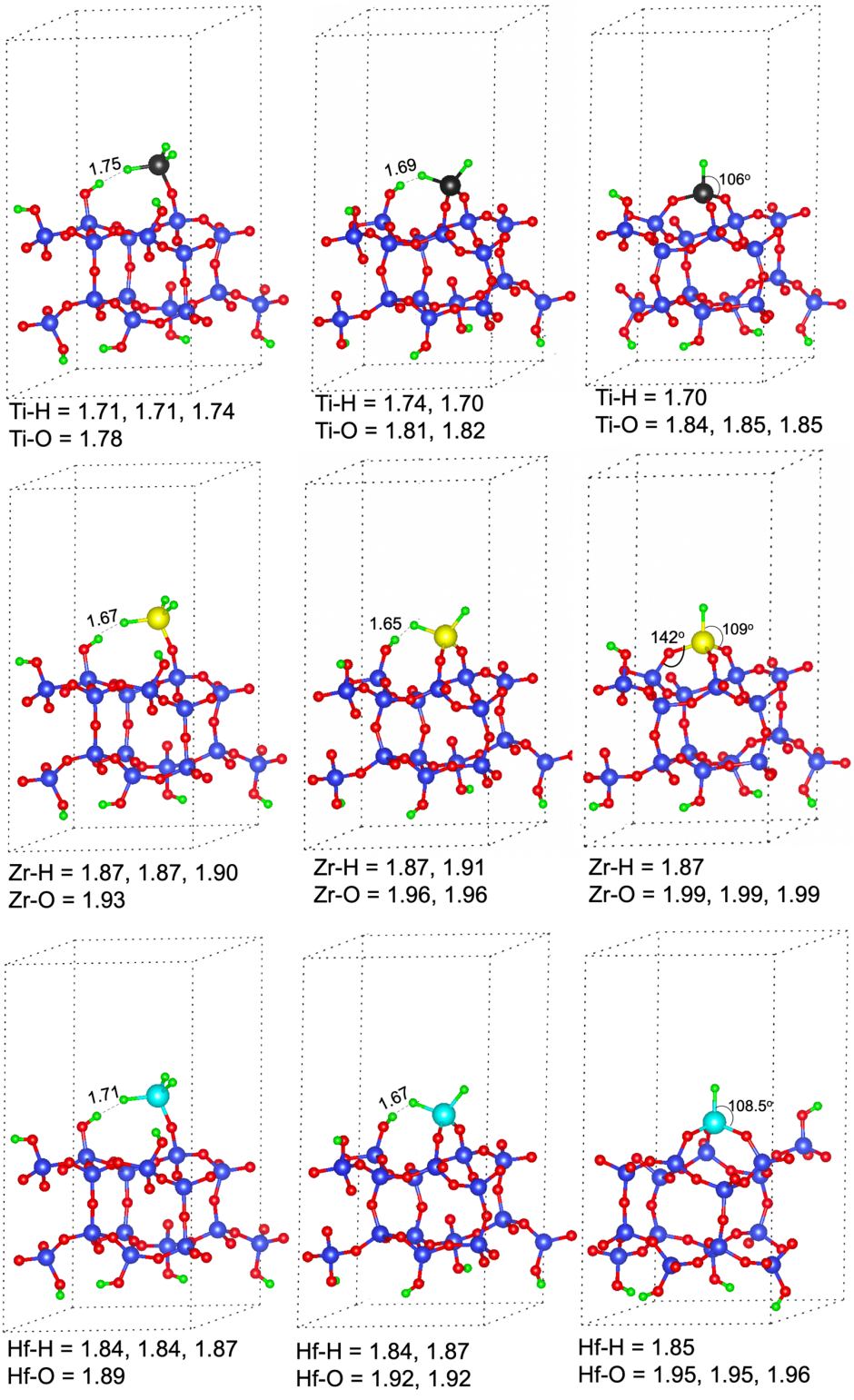

Fig. S5: Structures of $(\equiv SiO)_nM(H)_{4-n}$ on (111) silica. Top row for M=Ti, second row for M=Zr, and third row for M=Hf with n = 1, 2, 3 (from left to right). Atoms are colored as H: green, O: red, Si: blue, Ti : black (●), Zr : yellow (●), Hf : cyan (light blue, ●). All distances in Å. CONTCARs in Zenodo.[11]

3-4mr oligomerization intermediates and reactions

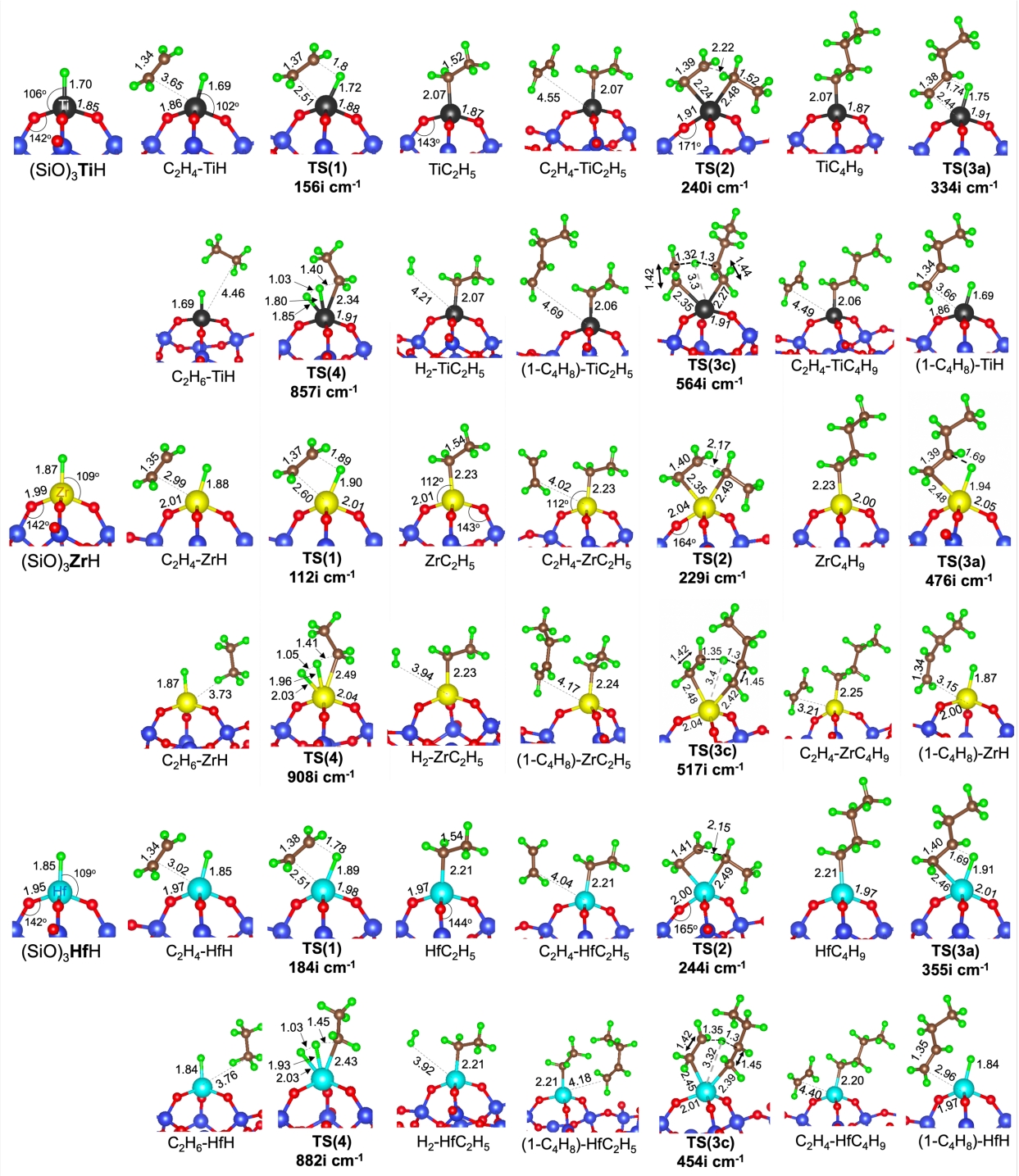

Fig. S6: Geometries of species formed along pathways shown in Fig. 2 on 3-4mr (≡SiO)$_3$MH site on periodic (111) silica surface. Top two rows show species for (≡SiO)$_3$**Ti**H, followed by two rows of (≡SiO)$_3$**Zr**H species and the last two rows for (≡SiO)$_3$**Hf**H species. Bond distances in Å and angles in degrees (°). CONTCARs in Zenodo.[11]

Table S6: M-O bond distances and O-M-O bond angles of intermediates formed along the $2C_2H_4 \rightarrow C_4H_8$ pathway on **3-4mr** ($\equiv SiO)_3MH$ site. $\overline{M-O}$ and $\overline{\angle OMO}$ are average distances and angles, respectively. Dihedral angle for transition state is between the atoms in which bond is formed or broken

Species	M-O (Å)			$\overline{M-O}$ (Å)	M-H or M-C(Å)	∠O-M-O (°)			$\overline{\angle OMO}$ (°)	∠Dihedral (°)
	M-O1	M-O2	M-O3			O1-M-O2	O2-M-O3	O3-M-O1		
Ti-H	1.84	1.85	1.85	1.85	1.7	112.4	112.8	112.5	112.6	
Zr-H	1.99	1.99	1.99	1.99	1.87	109.5	110.3	109.8	109.9	
Hf-H	1.95	1.95	1.96	1.95	1.85	110	110.9	110.4	110.4	
C_2H_4-TiH	1.84	1.86	1.85	1.85	1.69	111.7	113.2	112.2	112.4	
C_2H_4-ZrH	2	2	2.01	2.00	1.88	104.8	105.5	113.7	108.0	
C_2H_4-HfH	1.97	1.96	1.98	1.97	1.85	105.1	105.8	113.3	108.1	
TS1_Ti	1.87	1.87	1.88	1.87	1.72	105.4	105.4	118.4	109.7	4.7 (Ti-C-C-H)
TS1_Zr	2	2.01	2.01	2.01	1.9	103.7	104.1	114	107.3	4.1 (Zr-C-C-H)
TS1_Hf	1.97	1.97	1.99	1.98	1.89	103.7	103.8	114	107.2	3.9 (Hf-C-C-H)
TiC_2H_5	1.85	1.86	1.87	1.86	2.07*	112.3	113.3	112.9	112.8	
ZrC_2H_5	1.99	2	2.01	2.00	2.23*	110.9	111.6	110.5	111.0	
HfC_2H_5	1.96	1.97	1.97	1.97	2.21*	111.5	110.7	110.3	110.8	
C_2H_4-TiC_2H_5	1.86	1.87	1.86	1.86	2.07	113.0	112.2	113.4	112.9	
C_2H_4-ZrC_2H_5	2.01	1.99	2.0	2.0	2.23	110.9	109.7	110.7	110.4	
C_2H_4-HfC_2H_5	1.97	1.96	1.97	1.97	2.21	111.2	110.7	110.0	110.6	
TS2_Ti	1.88	1.88	1.91	1.89	2.24 **	116.3	100.6	100.4	105.8	24.3 (Ti-C-C-C)
TS2_Zr	2.03	2.02	2.04	2.03	2.35 **	118.8	98.2	97.2	104.7	18.5 (Zr-C-C-C)
TS2_Hf	1.99	1.99	2	1.99	2.32 **	115.9	98.3	99.2	104.5	24.7 (Hf-C-C-C)
TiC_4H_9	1.86	1.86	1.86	1.86	2.07 *	112.5	113.1	112.8	112.8	
ZrC_4H_9	2	2	2	2.00	2.23*	110.5	110.6	110	110.4	
HfC_4H_9	1.96	1.96	1.97	1.96	2.21*	110.7	111.2	110.5	110.8	
TS3a_Ti	1.87	1.91	1.87	1.88	1.75	103.3	105	119.1	109.1	11.8 (Ti-C-C-H)
TS3a_Zr	2	2	2.05	2.02	1.94	101.4	103.4	115.1	106.6	12.5 (Zr-C-C-H)
TS3a_Hf	1.96	1.97	2.01	1.98	1.91	102.6	104.0	113.7	106.8	9.5 (Hf-C-C-H)
C_4H_8-TiH	1.85	1.84	1.86	1.85	1.69	111.9	113.6	111.1	112.1	
C_4H_8-ZrH	1.98	2	2.0	1.99	1.87	105.8	113.9	105.9	108.5	
C_4H_8-HfH	1.95	1.97	1.97	1.96	1.85	104.6	105.7	114.5	108.3	
C_2H_4-TiC_4H_9	1.86	1.87	1.87	1.87	2.06	113.5	112.6	112.4	112.8	
C_2H_4-ZrC_4H_9	2.0	2.02	2.01	2.01	2.25	105.3	114.2	105.7	108.4	
C_2H_4-HfC_4H_9	1.97	1.97	1.96	1.97	2.20	110.1	111.0	110.8	110.6	
TS3c_Ti	1.89	1.91	1.84	1.88	2.27	112.7	112	99.9	108.2	

					(C of C_4H_8)					
TS3c_Zr	2.04	1.98	2.02	2.01	2.42	108.4	110.7	100.5	106.5	
TS3c_Hf	2.01	1.95	1.99	1.98	2.39	108.8	110.6	99.8	106.4	
C_4H_8-TiC_2H_5	1.86	1.86	1.86	1.86	2.06 *	113.6	112.8	112.7	113.0	
C_4H_8-ZrC_2H_5	2.0	2.01	2.0	2.0	2.24 *	109.4	111.4	108.7	109.8	
C_4H_8-HfC_2H_5	1.96	1.97	1.96	1.96	2.21 *	110.3	110.9	110.0	110.4	
H_2-TiC_2H_5	1.87	1.86	1.86	1.86	2.07 *	113.0	113.3	112.3	112.9	
H_2-ZrC_2H_5	2.01	2.0	2.0	2.0	2.23 *	110.7	111.2	109.5	110.5	
H_2-HfC_2H_5	1.95	1.98	1.96	1.96	2.21 *	111.4	110.0	110.7	110.7	
TS4_Ti	1.86	1.85	1.91	1.87	1.8#	116.8	107.0	104.7	109.5	6.9 (Ti-C-H-H)
TS4_Zr	1.99	1.99	2.04	2.01	1.96#	113.5	104.4	103.3	107.1	21.6 (Zr-H-C-C)
TS4_Hf	1.96	1.95	2.0	1.97	1.93#	112.6	105.0	103.3	107.0	0.5 (Hf-C-H-H)
C_2H_6-TiH	1.84	1.85	1.84	1.84	1.69	113.2	112.7	112.8	112.9	
C_2H_6-ZrH	1.98	2.0	1.99	1.99	1.87	109.2	111.5	108.2	109.6	
C_2H_6-HfH	1.95	1.96	1.96	1.96	1.84	110.0	111.6	109.0	110.2	

**: Bond distance is between M and carbon (C) of incoming ethylene that is nearest to M.
*: Bond distance is between M and C_α of alkyl chain attached to M.
#: Bond distance is between M and H being transferred to ethyl chain

Table S7: PBE computed (E^{DFT}) and zero-point (E^{ZPE}) energies in eV of intermediates on 3-4mr (≡SiO)$_3$MH site.

	(SiO)$_3$**Ti**H		(SiO)$_3$**Zr**H		(SiO)$_3$**Hf**H	
	E^{DFT}	E^{ZPE}	E^{DFT}	E^{ZPE}	E^{DFT}	E^{ZPE}
(SiO)$_3$MH (clean)	-439.705	0.248	-441.12	0.484	-443.153	0.209
C_2H_4--MH(SiO)$_3$	-471.708	1.628	-473.279	1.897	-475.253	1.621
TS(1)	-471.630	1.668	-473.165	1.898	-475.054	1.620
(SiO)$_3$MC_2H_5	-473.277	1.763	-474.574	2.008	-476.579	1.727
C_2H_4--MC_2H_5(SiO)$_3$	-505.310	3.138	-506.576	3.380	-508.576	3.109
TS(2) or TS(3b)	-503.827	3.212	-505.744	3.454	-507.525	3.176
(SiO)$_3$MC_4H_9	-506.334	3.276	-507.652	3.514	-509.658	3.235
TS(3a)	-504.683	3.150	-506.222	3.385	-508.161	3.112
1-C_4H_8--MH(SiO)$_3$	-504.922	3.133	-506.456	3.396	-508.418	3.123
C_2H_4--MC_4H_9(SiO)$_3$	-538.369	4.658	-539.663	4.898	-541.676	4.611
TS(3c)	-536.717	4.581	-538.413	4.824	-540.436	4.552
1-C_4H_8-MC_2H_5(SiO)$_3$	-538.531	4.652	-539.756	4.900	-541.781	4.629
H_2--MC_2H_5	-480.058	2.080	-481.359	2.321	-483.314	2.035
TS(4)	-479.044	2.173	-480.538	2.399	-482.501	2.118
MH--C_2H_6	-480.210	2.242	-481.655	2.484	-483.686	2.210

Table S8: ZPE corrected reactions (**dE**) and activation (E_a) energies in eV for ethylene dimerization on 3-4mr $(\equiv SiO)_3M(H)$. Non-activated adsorption steps are denoted by "*".

Name	Reactions	Ti		Zr		Hf	
		E_a	dE	E_a	dE	E_a	dE
1*	$C_2H_4(g) + MH \rightarrow C_2H_4\text{--}MH$	0	-0.01	0	-0.14	0	-0.08
1	$C_2H_4\text{--}MH \rightarrow MC_2H_5$	0.12	-1.43	0.12	-1.18	0.20	-1.22
2*	$C_2H_4(g) + MC_2H_5 \rightarrow C_2H_4\text{--}MC_2H_5$	0	-0.05	0	-0.02	0	-0.004
2	$C_2H_4\text{--}MC_2H_5 \rightarrow MC_4H_9$	1.56	-0.89	0.91	-0.94	1.12	-0.96
3a	$MC_4H_9 \rightarrow C_4H_8\text{--}MH$	1.52	1.27	1.30	1.08	1.37	1.13
3a*	$C_4H_8\text{--}MH \rightarrow 1\text{-}C_4H_8(g) + MH$	0	0.04	0	0.13	0	0.06
3c*	$C_2H_4(g) + MC_4H_9 \rightarrow C_2H_4\text{--}MC_4H_9$	0	-0.04	0	-0.02	0	-0.03
3c	$C_2H_4\text{--}MC_4H_9 \rightarrow MC_2H_5 + 1\text{-}C_4H_8(g)$	1.57	-0.10	1.18	-0.10	1.18	-0.09
4*	$H_2(g) + MC_2H_5 \rightarrow H_2\text{--}MC_2H_5$	0	0.03	0	0.02	0	0.06
4	$H_2\text{--}MC_2H_5 \rightarrow HM + C_2H_6(g)$	1.11	0.02	0.9	-0.1	0.90	-0.17

a)

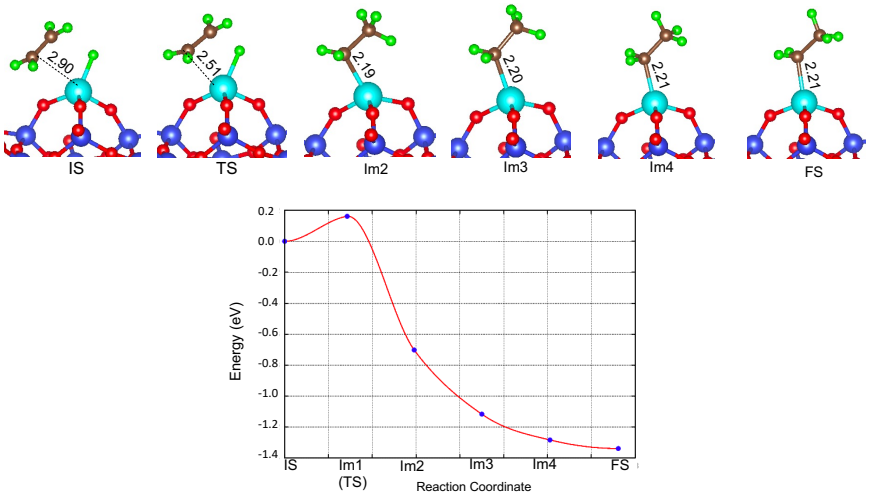
2.90
2.51
2.19
2.20
2.21
2.21
IS
TS
Im2
Im3
Im4
FS
Energy (eV)
Reaction Coordinate
IS
Im1 (TS)
Im2
Im3
Im4
FS

b)

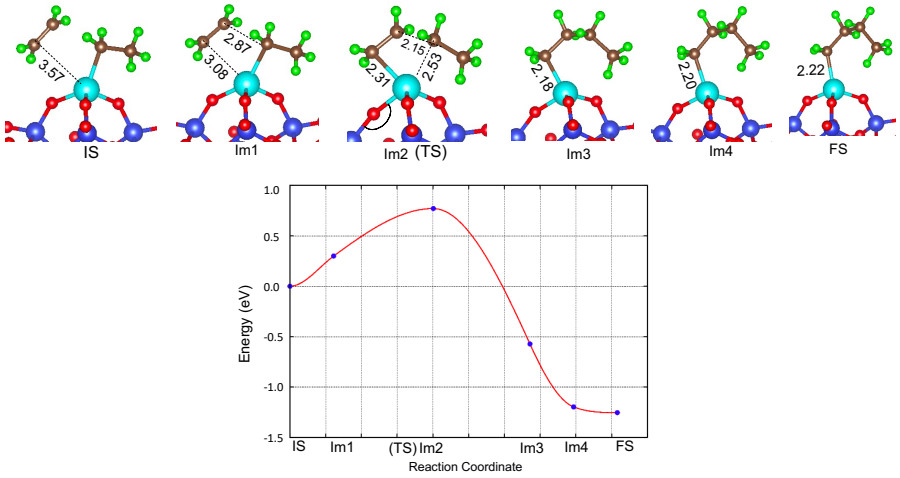
3.57
2.87
3.08
2.31
2.15
2.53
2.18
2.20
2.22
IS
Im1
Im2 (TS)
Im3
Im4
FS
Energy (eV)
Reaction Coordinate
IS
Im1
(TS) Im2
Im3
Im4
FS

c)

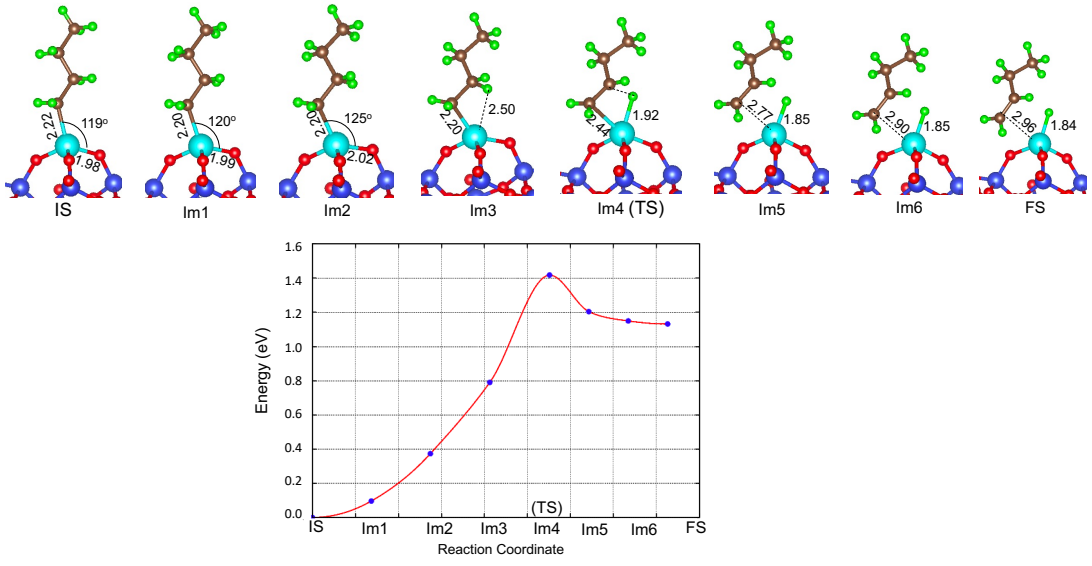
2.22
119°
1.98
2.20
120°
1.99
2.20
125°
2.02
2.20
2.50
2.44
1.92
2.77
1.85
2.90
1.85
2.96
1.84
IS
Im1
Im2
Im3
Im4 (TS)
Im5
Im6
FS
Energy (eV)
Reaction Coordinate
IS
Im1
Im2
Im3
Im4 (TS)
Im5
Im6
FS

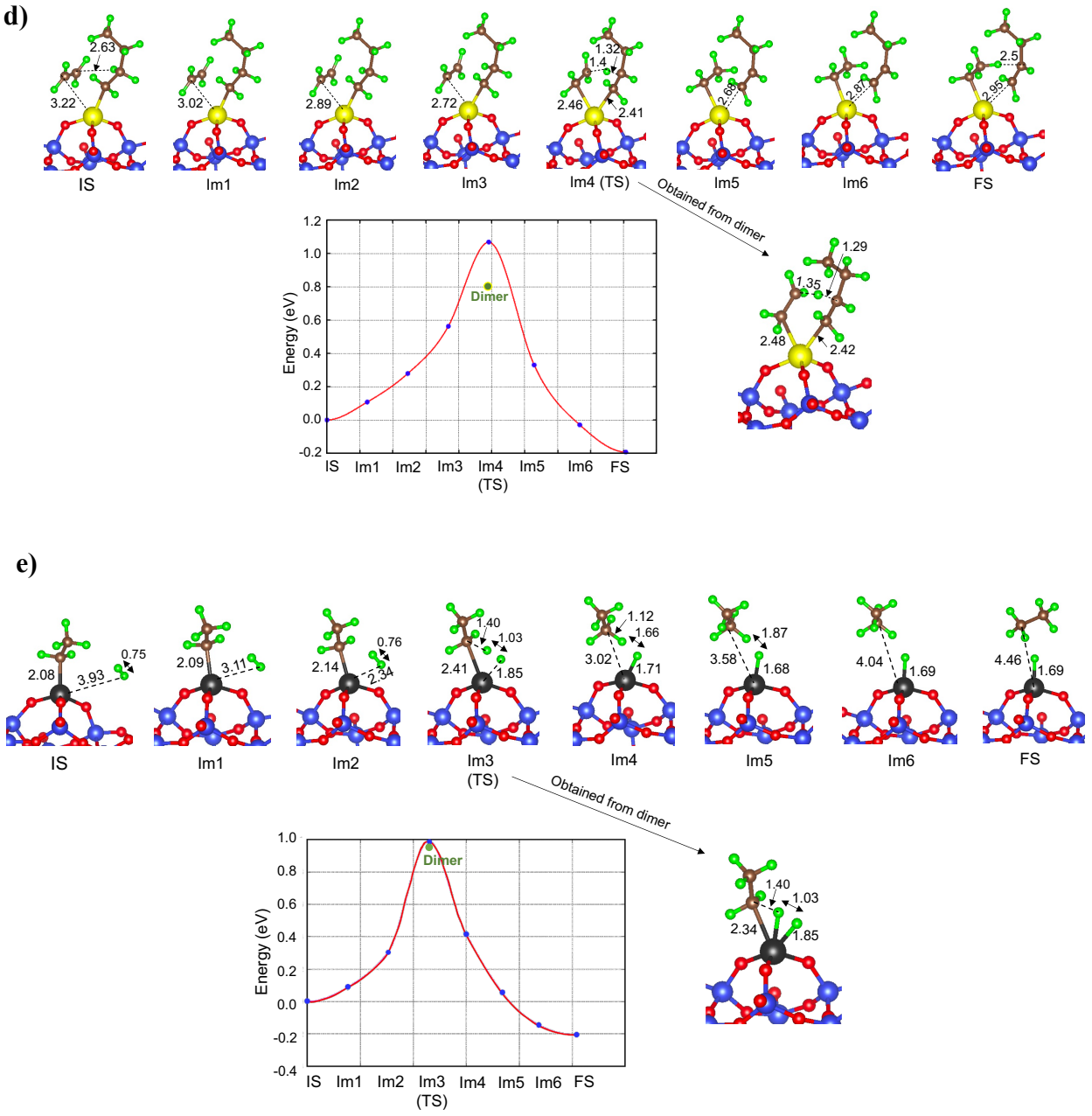

Fig. S7: Transition state search results on 3-4mr (SiO)3MH sites. **(a), (b), (c)** CI-NEB results for TS(1), TS(2), TS(3a), respectively, on $(\equiv SiO)_3HfH$ **(d)** CI-NEB and dimer results for TS(3c) on $(\equiv SiO)_3ZrH$. **(e)** CI-NEB and dimer results for TS(4) on $(\equiv SiO)_3TiH$.

3-4mr transition state distortions

Induced strain is measured by the average stretch, $\langle a \rangle$ generated in M-O-Si angle during transition from initial state (not to be a physiosorbed state) to TS where the most rearrangement occurs in the metal's coordination sphere and is calculated as

$$\langle a \rangle = \frac{\sum_{l=1}^{3} (a_l^{\dagger} - a_l)}{3}$$

a_l and $a_l^{\dagger}$ are M-O-Si angles in initial state (IS) and the leading TS. For instance, IS and TS pairs are $(\equiv SiO)_3MH$ and TS(1), $(\equiv SiO)_3MC_2H_5$ and TS(2), $(\equiv SiO)_3MC_4H_9$ and TS(3a), respectively. From Table S9, $\langle a \rangle$ is largest in TS(2) than in TS(3a) and TS(1). It is not precisely correlated to changes in activation barrier across Ti, Zr and Hf, but provides a summary about geometric distortion in TS relative to IS.

Table S9: M-O-Si bond angles (∠) and $\langle a \rangle$ in degrees (°) for 3-4mr $(\equiv SiO)_3MH$ site (M= Ti, Zr, Hf)

Species on 3-4mr silica(111)	∠Si-O-M (°)			$\overline{\angle SiOM}$ (°)	Average Induced Strain, <a> (°)	
	Si1-O1-M	Si2-O2-M	Si3-O3-M		IS → TS	<a> (°)
Ti-H	142.4	141.7	139.9	141.3		
Zr-H	141.8	141	139.1	140.6		
Hf-H	142.1	141.6	139.5	141.1		
TS1_Ti	148.1	143.9	140.1	144	TiH→TS1	144 -141.3 = 2.7
TS1_Zr	144.8	144.2	140.7	143.2	ZrH→TS1	143.2 - 140.6 = 2.6
TS1_Hf	145.8	144.9	142.3	144.3	HfH→TS1	144.3 - 141.1 = 3.2
TC_2H_5 (2)	143.3	137.1	140.4	140.3		
ZrC_2H_5 (2)	138.8	134.8	142.6	138.7		
HfC_2H_5 (2)	143.8	140.0	136.0	139.3		
TS2_Ti	171.2	139.4	139.7	150.1	**Ti**: 2→TS2	150.1 - 140.3 = 9.8
TS2_Zr	163.6	138.6	138.3	146.8	**Zr:** 2→TS2	146.8 - 138.7 = 8.1
TS2_Hf	165.1	140.2	139.9	148.4	**Hf:** 2→TS2	148.4 - 139.3 = 9.1
TiC_4H_9 (4)	141.3	140.2	138.9	140.1		
ZrC_4H_9 (4)	140.2	138.1	140.0	139.4		
HfC_4H_9 (4)	141.4	140.7	138.0	140.0		
TS3a_Ti	147.0	144.0	141.3	144.1	**Ti:** 4→TS3a	144.1 - 140.1 = 4.0
TS3a_Zr	147.3	141.4	141.2	143.3	**Zr:** 4→TS3a	143.3 - 139.4 = 3.9
TS3a_Hf	149.1	141.7	142.6	144.5	**Hf:** 4→TS3a	144.5 - 140.0 = 4.5

Entropy models

ASE's[10] IdealGasThermo and HarmonicThermo functions are used to calculate ideal gas entropy and entropy of surface species plus transition state species, respectively in the harmonic limit with rigid rotor approximation.

$$S_{total} = S^{o}_{trans} + S_{vibrational} + S_{rotational} + S_{electronic} \quad \text{(S.3)}$$

Translation entropy (S_{trans}) of ideal gas of molecular mass, m at standard pressure, P^{o} and temperature, T from Sackur-Tetrode Equation[8]

$$S^{o}_{trans} = k_B \left[ln \left[\left(\frac{2\pi m k_B T}{h^2} \right)^{\frac{3}{2}} \frac{k_B T}{P^{o}} \right] + \frac{5}{2} \right] \quad \text{(S.4)}$$

Where $k_B$is Boltzmann constant and h is Plank's constant. At 298 K and 475 K, $T.S^{o}_{trans,C2H4}$ is 0.464 eV and 0.784 eV, respectively, while $T.S^{o}_{trans,C4H8}$ is 0.491 eV and 0.826 eV, respectively.

$S_{electronic}$ = 0 as no spin degenerate ground states exist for any species

$$S_{vibrational} = k_B \sum_i \frac{h\upsilon_i}{k_B T} \left(\frac{1}{e^{\frac{h\upsilon_i}{k_B T}} - 1} \right) - k_B \sum_i \ln \left(1 - e^{-\frac{h\upsilon_i}{k_B T}} \right) \quad \text{(S.5)}$$

Being non-linear, they have 3N-6 real vibrational modes (υ_i), where N is the number of atoms in the gas molecule. Both ethylene and 1-butene are non-linear molecules with symmetry numbers of 4 and 1, respectively. For surface species with some atoms frozen, there should be 3N real modes and 3N-1 real modes of vibration for a transition state.

Additionally, for non-linear gas molecules,

$$S_{rotational} = k_B \left[\ln \left[\left(\frac{8\pi^2 k_B T}{h^2} \right)^{\frac{3}{2}} \frac{\sqrt{I_A I_B I_C}}{\sigma} \right] + 1 \right] \quad \text{(S.6a)}$$

Where $I_A I_B I_C$ is the product of inertia of a molecule, summed over all atoms of the molecule, σ denotes the "rotational symmetry number" for the molecule.

While for linear gas molecules like hydrogen,

$$S_{rotational} = k_B \left[\ln \left(\frac{8\pi^2 I k_B T}{\sigma h^2} \right) + 1 \right] \quad \text{(S.6b)}$$

3-4mr free energy surfaces

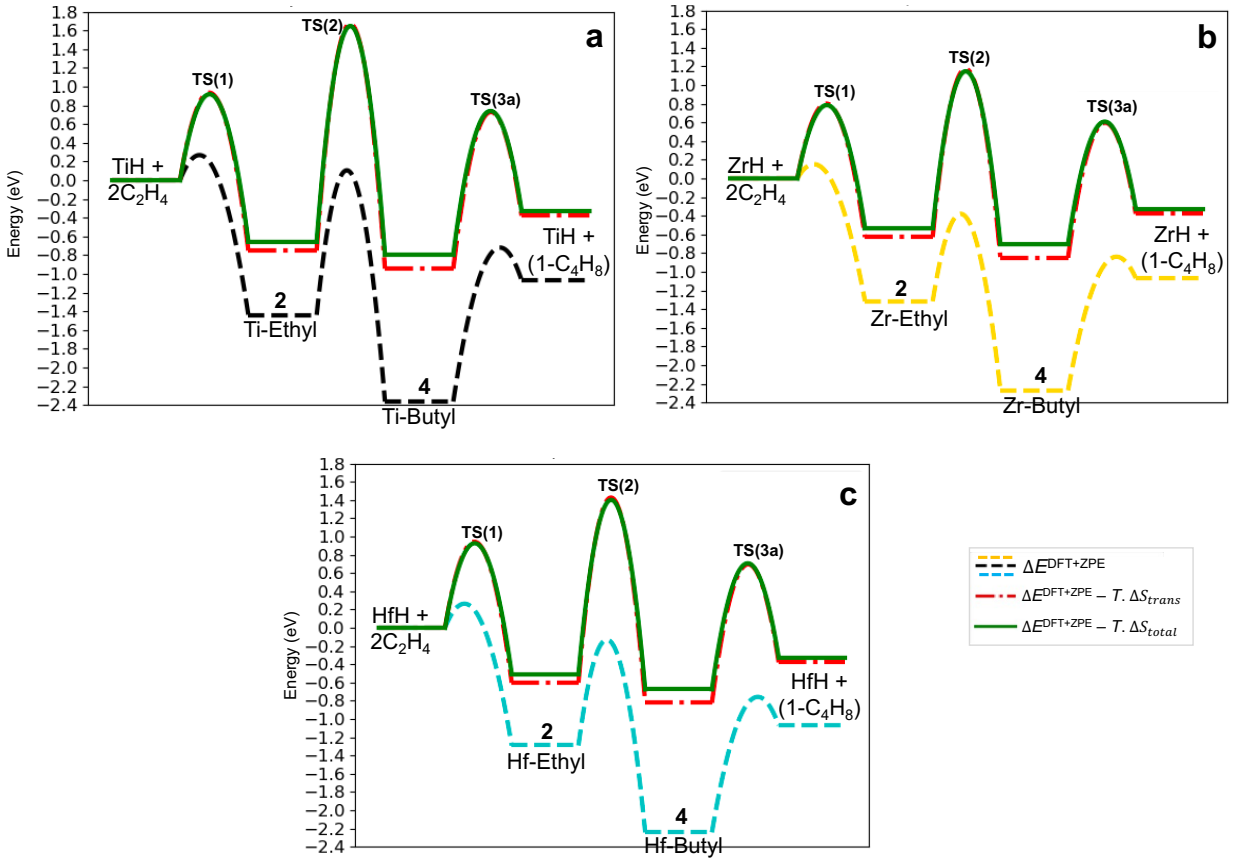

Fig. S8: Energy profiles of $2C_2H_4 \rightarrow 1\text{-}C_4H_8$ on 3-4mr $(\equiv SiO)_3M(H)$ sites of **a) Ti, b) Zr** and **c) Hf**. ZPE corrected electronic energy profile (dashed lines): Ti (black), Zr (yellow) and Hf (blue). Red (dot dashed) and green (solid) curves are the free energies at $T = 473$ K, $P = 1$ bar with either **1)** complete loss of translational entropy (S_{trans}) of gas molecule on reacting with surface, while retaining rotational and vibrational entropy (red curve) **2)** from harmonic vibrational modes of surface species combined with rigid rotor approximation (S_{total})(green curve). Physiosorbed states are excluded from this comparison.

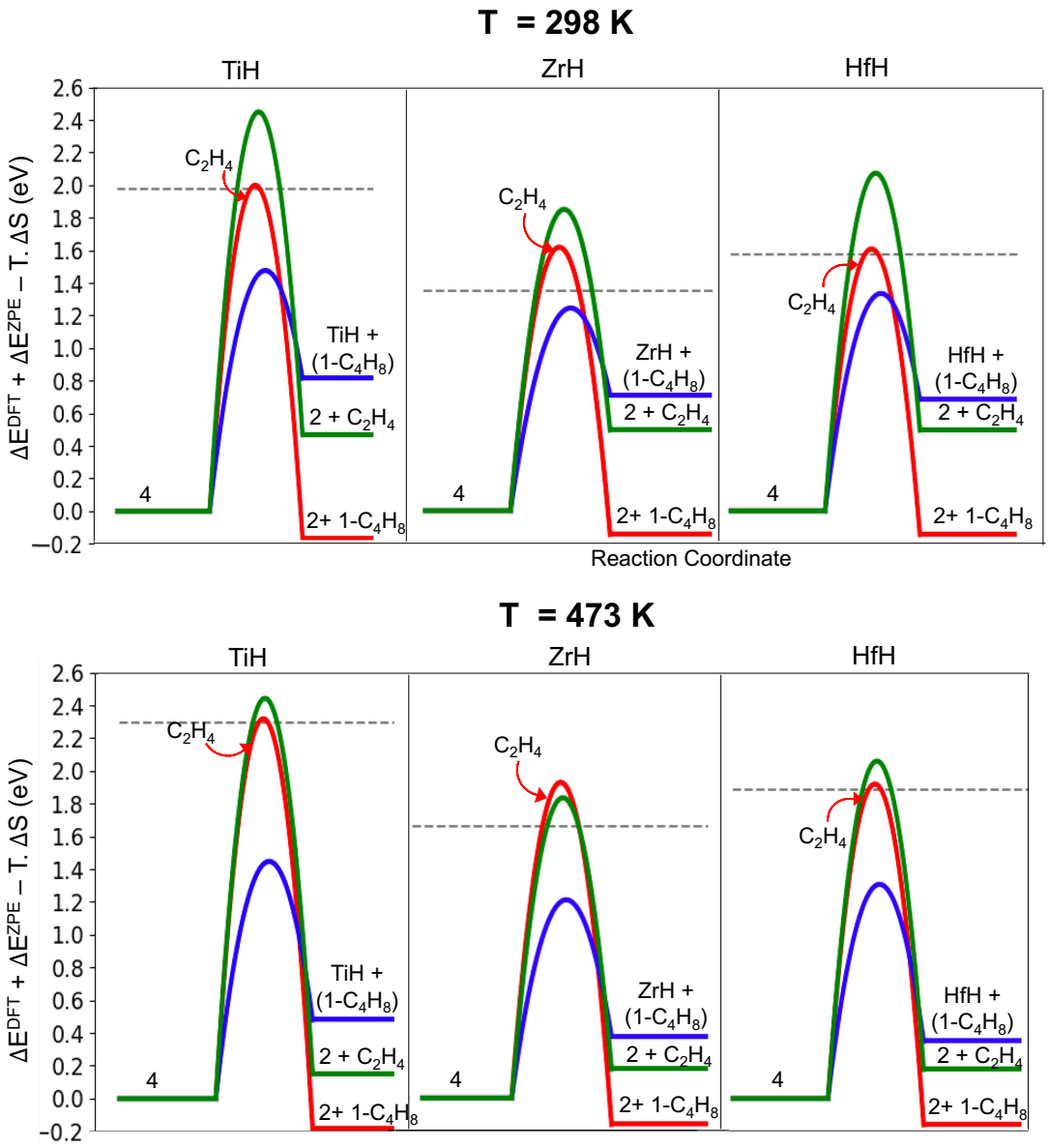

Fig. S9: PES of termination routes at $T = 298$ K and $T = 473$ K, $P = 1$ bar on the 3-4mr $(\equiv SiO)_3MC_4H_9$ sites on silica (111). Termination routes are color coded as in Fig. 4: β-H to M (blue curve, via TS(3a)), β-alkyl transfer to M (green curve) and β-H transfer to ethylene (red curve). Dashed line is energy barrier associated with chain growth via TS(2).

3-4mr microkinetic models

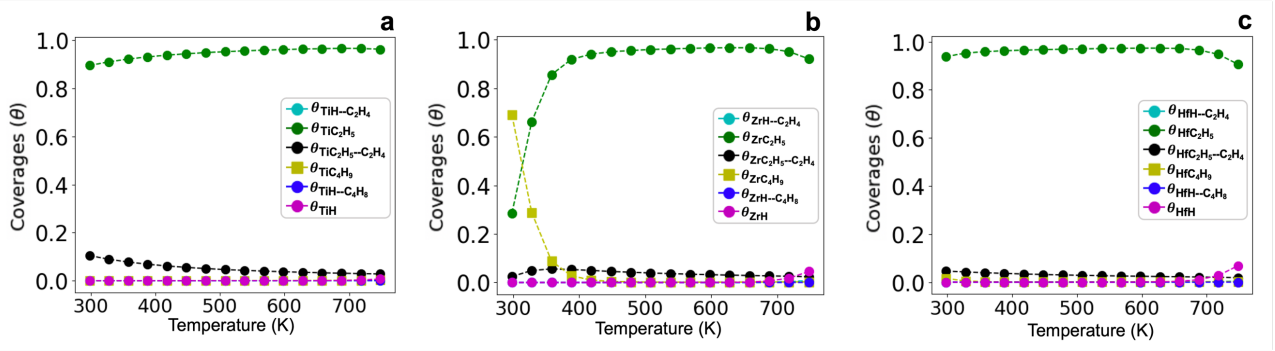

Fig. S10: Steady state coverages for 3-4mr (≡SiO)$_3$MH site of **a)** Ti, **b)** Zr and **c)** Hf against temperature at P_{C2H4} =17 bar.

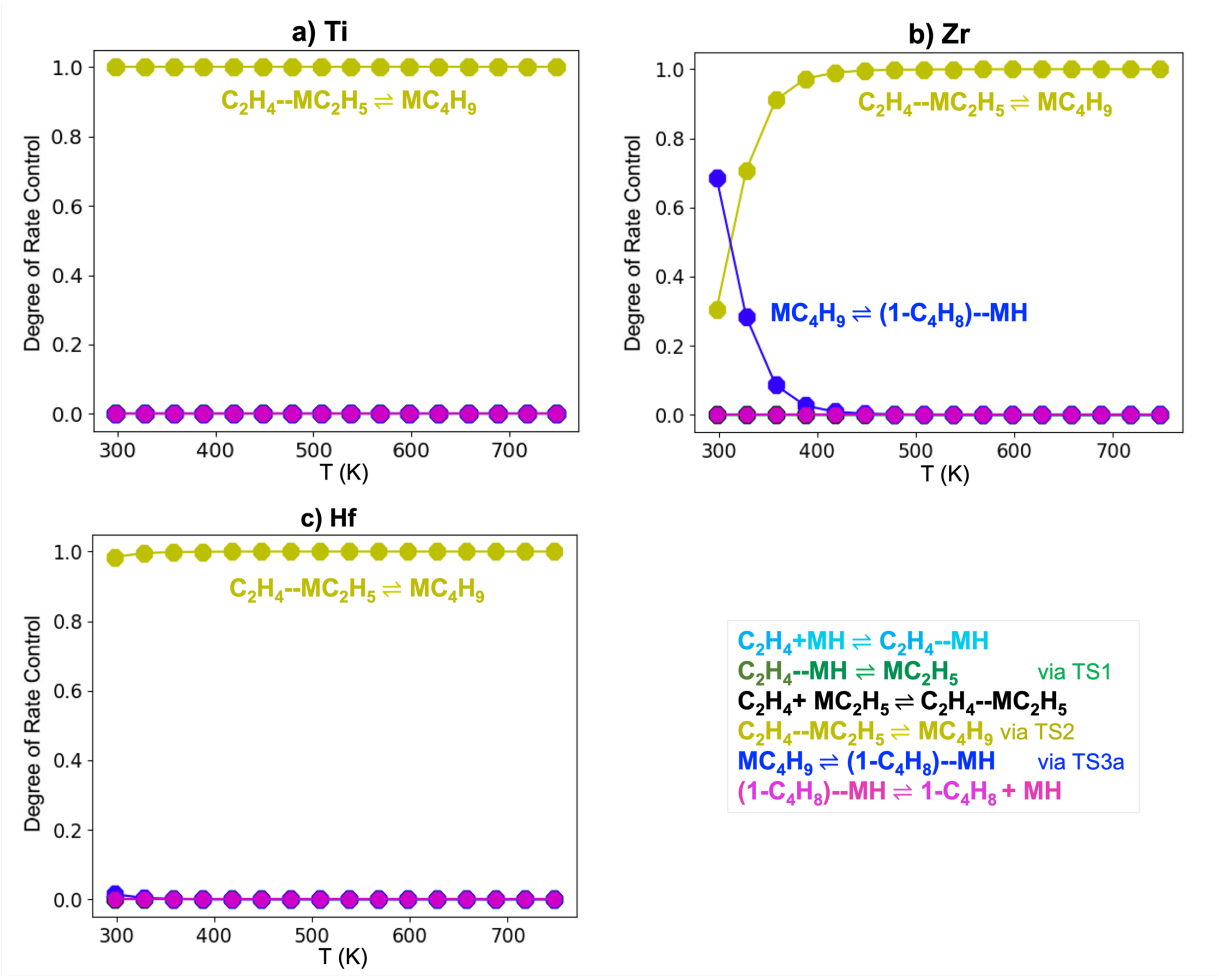

Fig. S11: Degree of rate control at P_{C2H4} =17 bar on **a)** Ti **b)** Zr and **c)** Hf 3-4mr (≡SiO)$_3$MH site. Reactions are color coded as shown.

Degree of Polymerization ($\overline{P_n}$)

Number average molecular weight M_n is calculated by equation (S.7a). M_i is the molecular weight of grown hydrocarbon chain composed of "i" monomer units. N_i is the number of chains having that molecular weight. M_o is the molecular weight of ethylene monomer.

We express the rate of production of N_i (eq. S.7a) as the rate of chain termination from surface species having identical monomer units or its coverage θ_i, where k_{term} is the termination rate constant.

$$M_n = \frac{\Sigma M_i.N_i}{\Sigma N_i} = \frac{\Sigma (i\, M_o).N_i}{\Sigma N_i} \quad \text{(S.7a)}$$

$$M_n = \frac{M_o \Sigma_{i=1}^{\infty} i.(k_{term}\theta_i)}{\Sigma\, k_{term}.\theta_i} \quad \text{(S.7b)}$$

Assuming, C-C bond formation step by migratory insertion into M-C bond and termination to be irreversible and rate constants k_{cc}, k_{term} remaining same for oligomers of all chain lengths, coverage of every surface species is expressed in terms of its predecessor[7] and a constant (α). α is probability of propagation in Cossee-Arlman mechanism.

$$\text{For } i > 1, \qquad \theta_i = \alpha\theta_{i-1} = \alpha^{i-1}.\theta_1 \quad \text{(S.8)}$$

Upon simplifying eq. S.7b by substituting eq. S.8, $\overline{P_n}$ can be calculated from eq S.9[7]

$$\overline{P_n} = \frac{M_n}{M_o} = \frac{1}{(1-\alpha)} \quad \text{(S.9)}$$

In $\overline{P_n}$ calculation, physisorption step is not considered and M-C insertion takes place as MP_{i-1}+ C_2H_4 → MP_i. MP_i is surface species composed of hydrocarbon chain of "i" monomer units bonded to metal site.

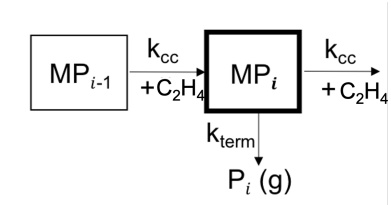

At steady state, by mole balance

$$MP_i = \frac{P_{C2H4}.k_{cc}}{(P_{C2H4}.k_{cc} + k_{term})} MP_{i-1} \quad \text{(S.10)}$$

$$\alpha = \frac{P_{C2H4}.k_{cc}}{(P_{C2H4}.k_{cc} + k_{term})} \quad \text{(S.11)}$$

With hydrogen present,

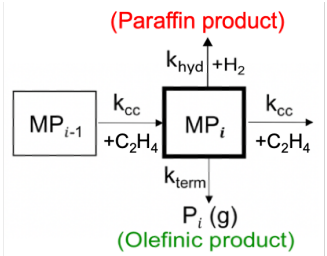

By steady state mole balance, $MP_i = \frac{P_{C2H4}.k_{cc}}{(P_{C2H4}.k_{cc} + k_{term} + P_{H2}.k_{hyd})} MP_{i-1}$

$$\overline{P_n} = \frac{1}{(1-\alpha_{H2})} = \frac{1}{(1-\frac{P_{C2H4}.k_{cc}}{P_{C2H4}.k_{cc} + k_{term} + P_{H2}.k_{hyd}})} = 1 + \frac{P_{C2H4}.k_{cc}}{k_{term} + P_{H2}.k_{hyd}} \quad \text{(S.12)}$$

Kinetic parameters, k_{cc} from 2→TS(2), k_{term} from 4 to TS(3a) , k_{hyd} is hydrogenolysis rate constant.

Low pressure and temperature rates and $\overline{P_n}$ for Zr site models

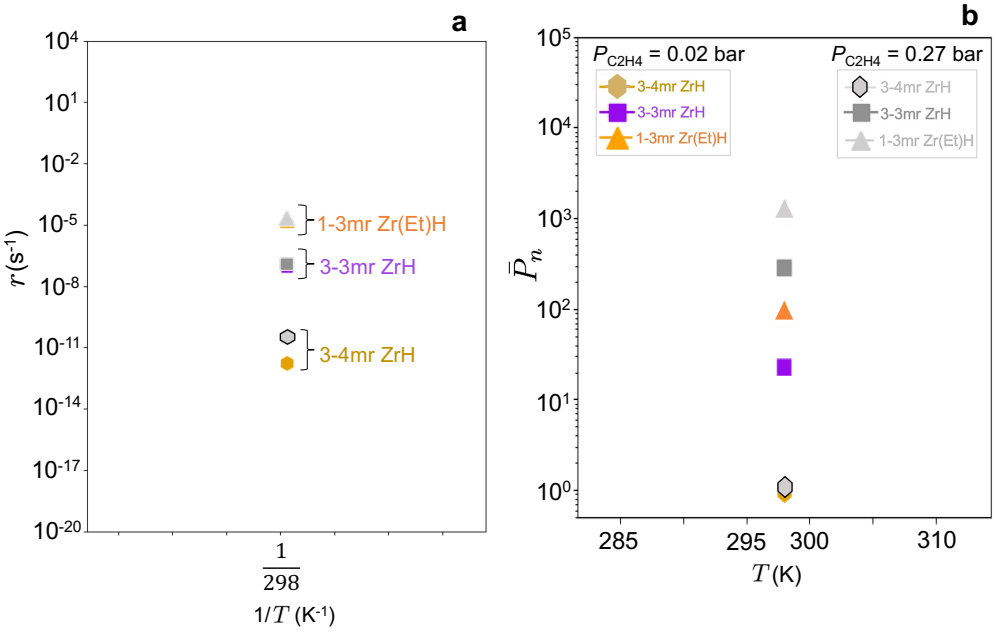

Fig. S12: (a) Computed rates, *r* and **(b)** degree of polymerization on model ZrH sites at P_{C2H4}= 0.02 bar (colored points) and 0.27 bar (grayscale points)

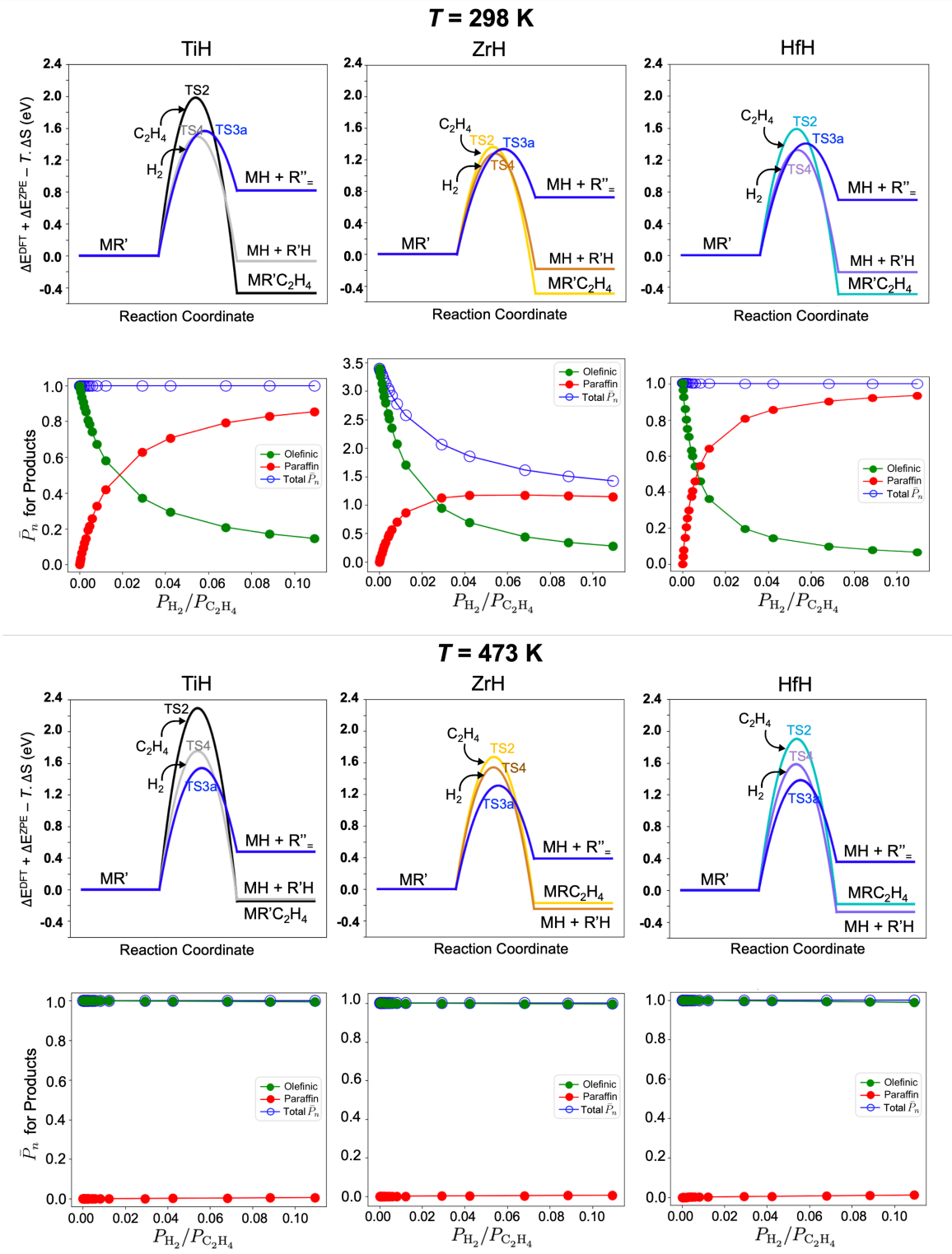

Fig. S13: (top) Free energy profiles for competing M-alkyl (MR') reaction on Ti, Zr, and Hf 3-4mr sites at 298 K. (second row) $\overline{P_n}$ against H_2/C_2H_4 molar ratio at 298 K. Third and fourth rows, same results at 473 K. Reactions shown are: **1)** M-C insertion via TS(2), **2)** hydrogenolysis to alkane (R'H) via TS(4) and **3)** termination by β-H to M via TS(3a) to olefin ($R^{"}_{=}$).

Grafting and hydrogenolysis of $Zr(CH_3)_4$ to 3-3mr site

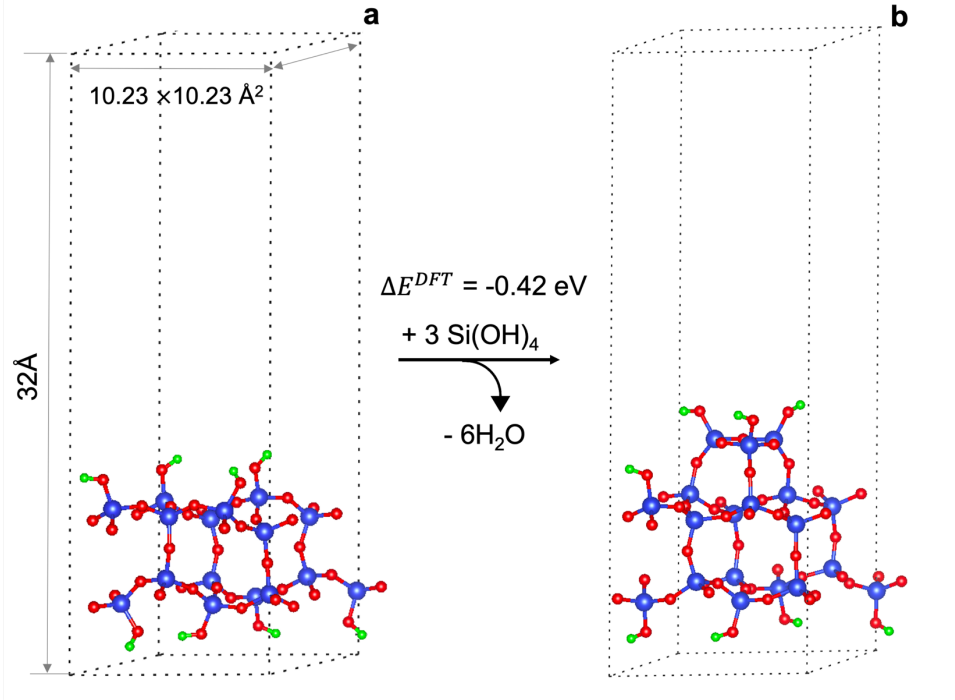

Fig. S14: Generation of reconstructed silica **(**in **b)** from functionalization of silica (111) facet (in **a**).

Grafting of precursor $Zr(CH_3)_4$ on silanols of reconstructed silica surface (Fig. S14b) is performed as per reaction (s1) to form $(\equiv SiO)_nZr(CH_3)_{4-n}$ species on surface, where n=1, 2 or 3. The transformation of these grafted Zr-alkyls to corresponding hydrides occurs as per reactions (s2). Structures of $(\equiv SiO)_nZr(CH_3)_{4-n}$, and $(\equiv SiO)_nZr(H)_{4-n}$ are in Fig. S16, in top row and bottom row, respectively with their energies in Table S10. Thermodynamics of sequential grafted complexes and their hydrogenation is shown in Fig. S15a with reaction energies in Table S11. Fig. S15b is a parity plot comparing heats of grafting (ΔE_{rxn}^{DFT}) of $Zr(CH_3)_4$ on reconstructed silica against the original silica(111) model.

Table S10: PBE computed energies (E^{DFT}) in eV of grafting and hydrogenolysis structures on reconstructed silica.

Species	**n**	E^{DFT} **(eV)**
$(\equiv SiO)M(CH_3)_3$	1	-573.702
$(\equiv SiO)_2M(CH_3)_2$	2	-551.044
$(\equiv SiO)_3M(CH_3)$	3	-527.632
$(\equiv SiO)M(H)_3$	1	-522.341
$(\equiv SiO)_2M(H)_2$	2	-516.885
$(\equiv SiO)_3M(H)$	3	-510.564
Clean Silica slab		-508.103

Table S11: PBE-computed heats of grafting $(CH_3)_4Zr$ in eV on reconstructed silica surface

M	Grafting $Zr(CH_3)_4$			Hydrogenolysis of grafted $(SiO)_nZr(CH_3)_{4-n}$		
	Calculated by reaction (s1)			Calculated by reaction (s2)		
	n=1	n=2	n=3	n=1	n=2	n=3
Zr on reconstructed silica	-2.17	-3.54	-4.16	-0.45	-0.38	-0.20
Zr on silica (111) (from Table S3)	-2.27	-4.21	-5.81	-0.62	-0.56	-0.21

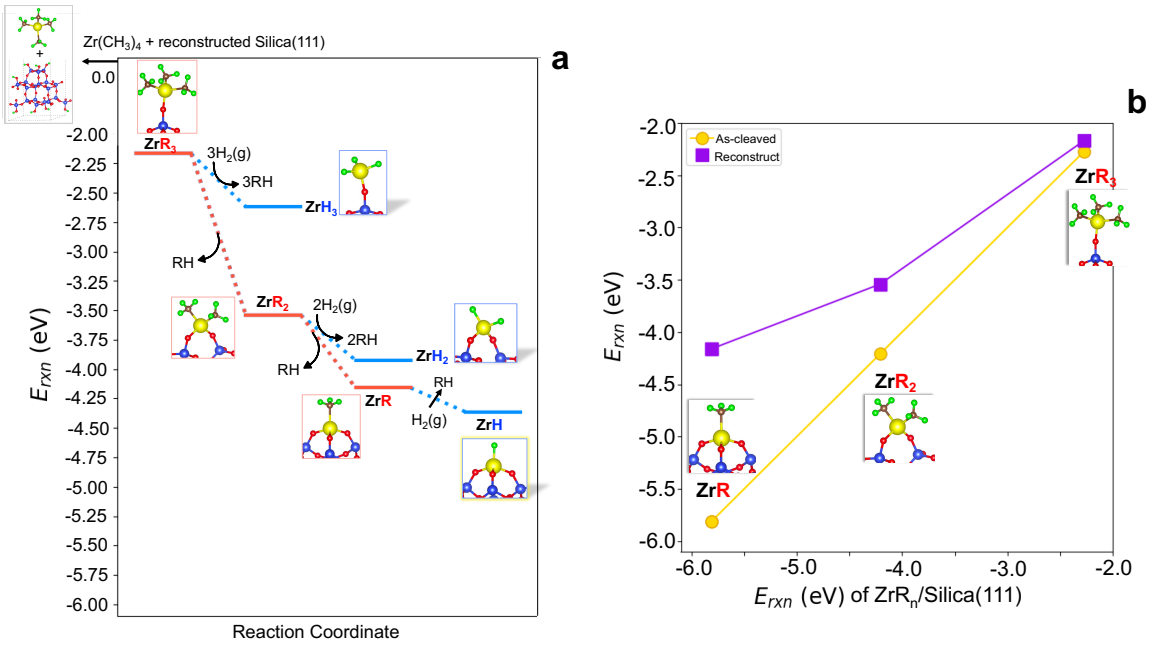

Fig. S15: a) Grafting and hydrogenolysis of $Zr(CH_3)_4$ on reconstructed silica(111) **b)** Parity plot of $Zr(CH_3)_4$ grafting energies on reconstructed silica vs parent/as-cleaved silica (111). Parity line shown in yellow.

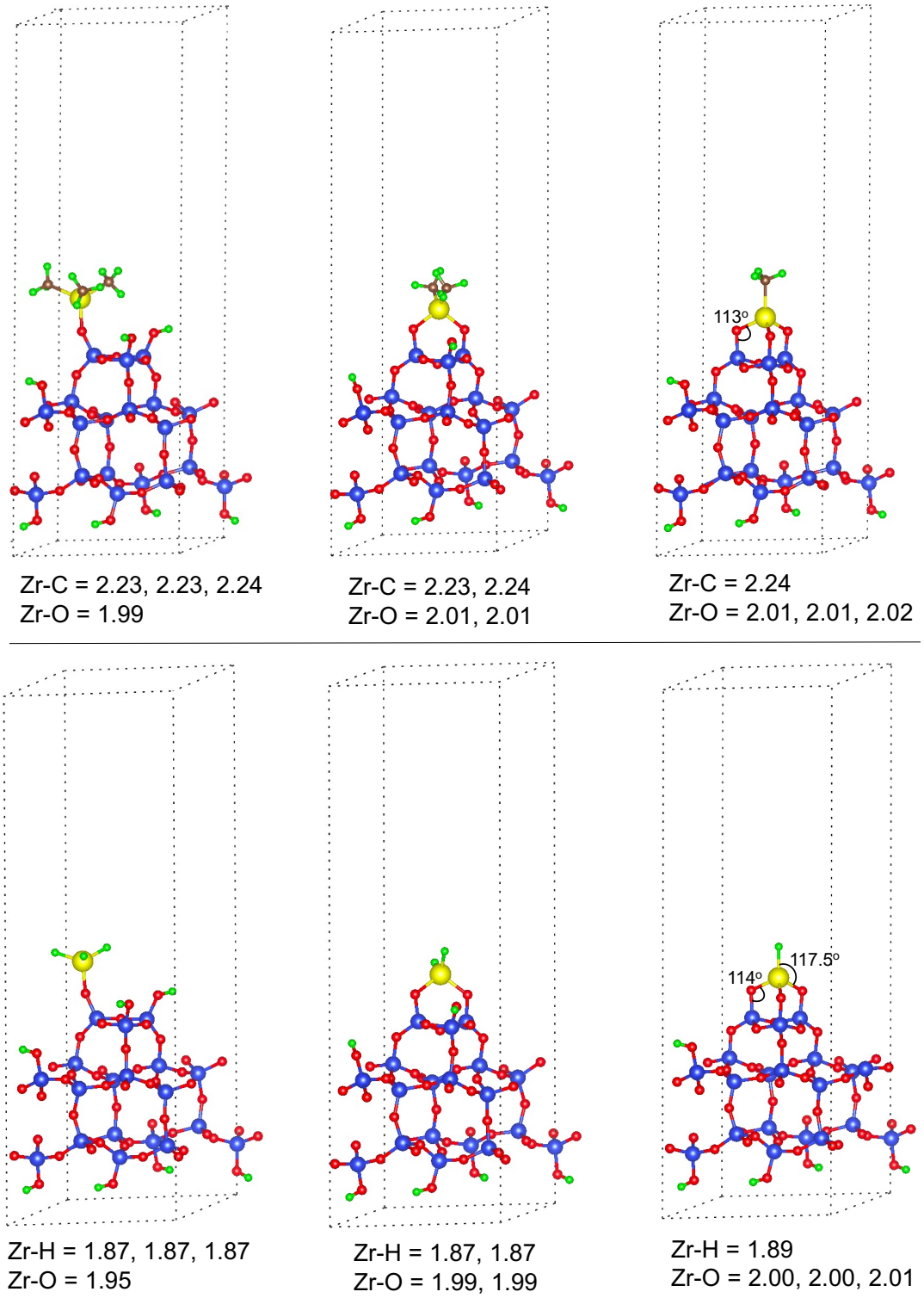

Fig. S16: Grafting and hydrogenolysis intermediates on reconstructed silica. H: green, C: brown, O: red, Si: blue, Zr: yellow (●). Distances in Å. CONTCARs in Zenodo.[11]

3-3mr oligomerization intermediates and reactions

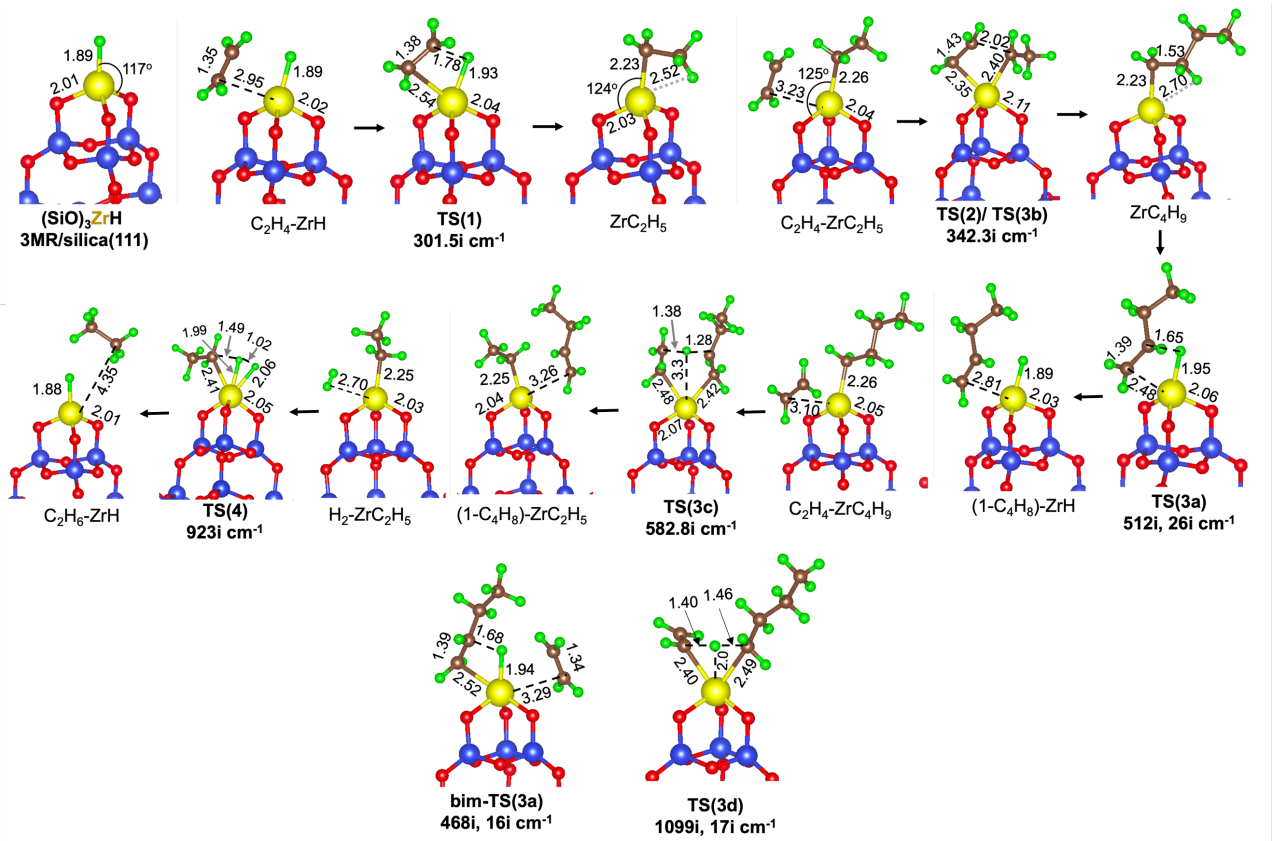

Fig. S17: Oligomerization intermediates on 3-3mr (≡SiO)$_3$**Zr**H site. Distances in Å. CONTCARs in Zenodo.[11]

Table S12: Structural parameters of species formed along pathways in Fig. 2 for $2C_2H_4 \rightarrow C_4H_8$ and $C_2H_4 + H_2 \rightarrow C_2H_6$ on 3-3mr $(\equiv SiO)_3ZrH$ site. **M-O** (Å) is bond distance between M and nearest O atoms. $\overline{M-O}$ is the average M-O bond distance and is calculated by: $\overline{M-O} = \frac{(M-O1)+(M-O2)+(M-O3)}{3}$. Similarly, $\angle\overline{OMO}$ is the average O-M-O angle (∠) in degrees (°). Dihedral angle is between atoms in which bond is formed or broken during transition state

Species	M-O (Å)			$\overline{M-O}$ (Å)	Smallest M-H or M-C(Å)	∠O-M-O (°)			$\angle\overline{OMO}$ (°)	∠Dihedral (°)
	M-O1	M-O2	M-O3			O1-M-O2	O2-M-O3	O3-M-O1		
Zr-H	2.01	2.01	2.01	2.01	1.89	100.3	100.4	100.7	100.5	
C_2H_4-ZrH	2.02	2.02	2.01	2.02	1.89	103.3	97.0	96.6	99.0	
TS1_Zr	2.02	2.01	2.04	2.02	1.93	103.9	95.8	95.7	98.5	9.8
ZrC_2H_5	2.03	2.02	2.02	2.02	2.23	100.3	102.0	100.2	100.8	
C_2H_4-ZrC_2H_5	2.02	2.02	2.04	2.03	2.26	97.2	96.4	105.6	99.7	
TS2 or TS3b	2.11	2.01	2.01	2.04	2.35	102.2	93.2	93.2	96.2	10.2
ZrC_4H_9	2.02	2.02	2.02	2.02	2.23	100.8	101.9	100.5	101.1	
TS3a_Zr	2.06	2.02	2.01	2.03	1.95	105.5	94.5	94.1	98.0	12.4
C_4H_8-ZrH	2.02	2.03	2.01	2.02	1.89	104.2	95.7	96.4	98.8	
C_2H_4-ZrC_4H_9	2.03	2.01	2.05	2.03	2.26	105.5	97.6	96.2	99.8	
TS3c_Zr	2.07	2.00	2.02	2.03	2.42 (C of C_4H_8)	101.3	96.6	95.4	97.8	
C_4H_8-ZrC_2H_5	2.03	2.01	2.04	2.03	2.25	98.6	98.1	103.2	100.0	
H_2-ZrC_2H_5	2.02	2.03	2.02	2.02	2.25	99.6	102.3	99.6	100.5	
TS4_Zr	2.05	2.02	2.01	2.03	1.99 (H of H_2)	100.5	94.3	98.1	97.6	21.7 (Zr-H-H-C)
C_2H_6-ZrH	2.01	2.0	2.0	2.0	1.88	100.7	100.2	99.9	100.3	

Table S13: PBE computed (E^{DFT}) and zero-point (E^{ZPE}) energies of 3-3mr (≡SiO)$_3$ZrH intermediates.

M = Zr	3-3mr (SiO)$_3$**Zr**H	
	E^{DFT} (eV)	E^{ZPE} (eV)
(SiO)$_3$MH (clean)	-510.525	0.484
C_2H_4--MH(SiO)$_3$	-542.872	1.892
TS(1)	-542.730	1.887
(SiO)$_3$MC_2H_5	-544.006	1.993
C_2H_4--MC_2H_5(SiO)$_3$	-576.151	3.399
TS(2) or TS(3b)	-575.539	3.444
(SiO)$_3$MC_4H_9	-577.098	3.512
TS(3a)	-575.800	3.385
C_4H_8--MH(SiO)$_3$	-576.008	3.393
C_2H_4--MC_4H_9(SiO)$_3$	-609.258	4.917
TS(3c)	-608.057	4.825
C_4H_8-MC_2H_5(SiO)$_3$	-609.290	4.898
H_2--MC_2H_5	-550.821	2.348
TS(4)	-550.112	2.383
MH--C_2H_6	-551.061	2.478
Bim-TS(3a)	-607.976	4.788
TS(3d)	-608.101	4.819
ZrC_2H_3	-535.719	1.401

Table S14: ZPE corrected reactions energies (**dE**) and activation energies ($\mathbf{E_a}$) in eV for ethylene dimerization on 3-3mr (≡SiO)$_3$Zr(H) site on reconstructed silica. Physisorption denoted by "*". For non-activated adsorption, barriers are assumed to be 0

No.	**Reactions**	**Zr**	
		$\mathbf{E_a}$	**dE**
1*	$\mathbf{C_2H_4 + MH \rightarrow C_2H_4\text{--}MH}$	0	-0.33
1	$\mathbf{C_2H_4\text{--}MH \rightarrow MC_2H_5}$	0.14	-1.03
2*	$\mathbf{C_2H_4 + MC_2H_5 \rightarrow C_2H_4\text{--}MC_2H_5}$	0	-0.13
2	$\mathbf{C_2H_4\text{--}MC_2H_5 \rightarrow MC_4H_9}$	0.66	-0.83
3a	$\mathbf{MC_4H_9 \rightarrow C_4H_8\text{--}MH}$	1.17	0.97
3a*	$\mathbf{C_4H_8\text{--}MH \rightarrow 1\text{-}C_4H_8 + MH}$	0	0.27
3c*	$\mathbf{C_2H_4 + MC_4H_9 \rightarrow C_2H_4\text{--}MC_4H_9}$	0	-0.14
3c	$\mathbf{C_2H_4\text{--}MC_4H_9 \rightarrow MC_2H_5 + 1\text{-}C_4H_8}$	1.11	-0.05
3d	$\mathbf{C_2H_4\text{--}MC_4H_9 \rightarrow MC_2H_3 + C_4H_{10}}$	1.06	-0.01
4	$\mathbf{H_2 + MC_2H_5 \rightarrow HM + C_2H_6}$	0.77	-0.06

3-3mr transition state distortions

We compared the C-C bond formation from M-C insertion and β-H termination barriers for the 3-4mr and 3-3mr (≡SiO)$_3$ZrH sites in Fig. 8b. Barriers are lower on the latter site, and the effect is more significant for the C-C bond formation via M-C insertion reaction. Greater H-M-O angles at the more strained 3-3mr site are consistent with more ready access of ethylene. Similar, smaller average distortion ⟨a⟩ at the transition state is consistent with lower barriers.

Table S15: Structural parameters of species formed on 3-4mr and 3-3mr (≡SiO)$_3$ZrH site on as-cleaved and reconstructed silica (111), respectively. Bond distances in angstroms (Å) and angles (∠) in degrees (°)

	3-4mr				3-3mr			
	∠Si-O-M (°)			$\overline{\angle SiOM}$ (°)	∠Si-O-M (°)			$\overline{\angle SiOM}$ (°)
Species	Si1-O1-M	Si2-O2-M	Si3-O3-M		Si1-O1-M	Si2-O2-M	Si3-O3-M	
Zr-H	141.8	141	139.1	140.6	113.2	113.3	113.2	113.2
TS1_Zr	144.8	144.2	140.7	143.2	116.7	114.1	113.8	114.9
ZrC_2H_5 (2)	138.8	134.8	142.6	138.7	112.0	111.9	112.9	112.3
TS2_Zr	163.6	138.6	138.3	146.8	117.5	116.9	116.2	116.9
ZrC_4H_9 (4)	140.2	138.1	140.0	139.4	111.8	111.9	112.7	112.1
TS3a_Zr	147.3	141.4	141.2	143.9	113.8	117.4	114.3	115.2
	Average Induced Strain, <a> (°)							
Zr: ZrH→TS1	143.2- 140.6 = 2.6				114.9 -113.2 = 1.7			
Zr: 2→TS2	146.8 - 139.2 = 8.1				112.3 - 116.9 = 4.6			
Zr: 4→TS3a	143.9 - 139.4 = 4.5				115.2 – 112.1 = 3.1			

3-3mr microkinetic model

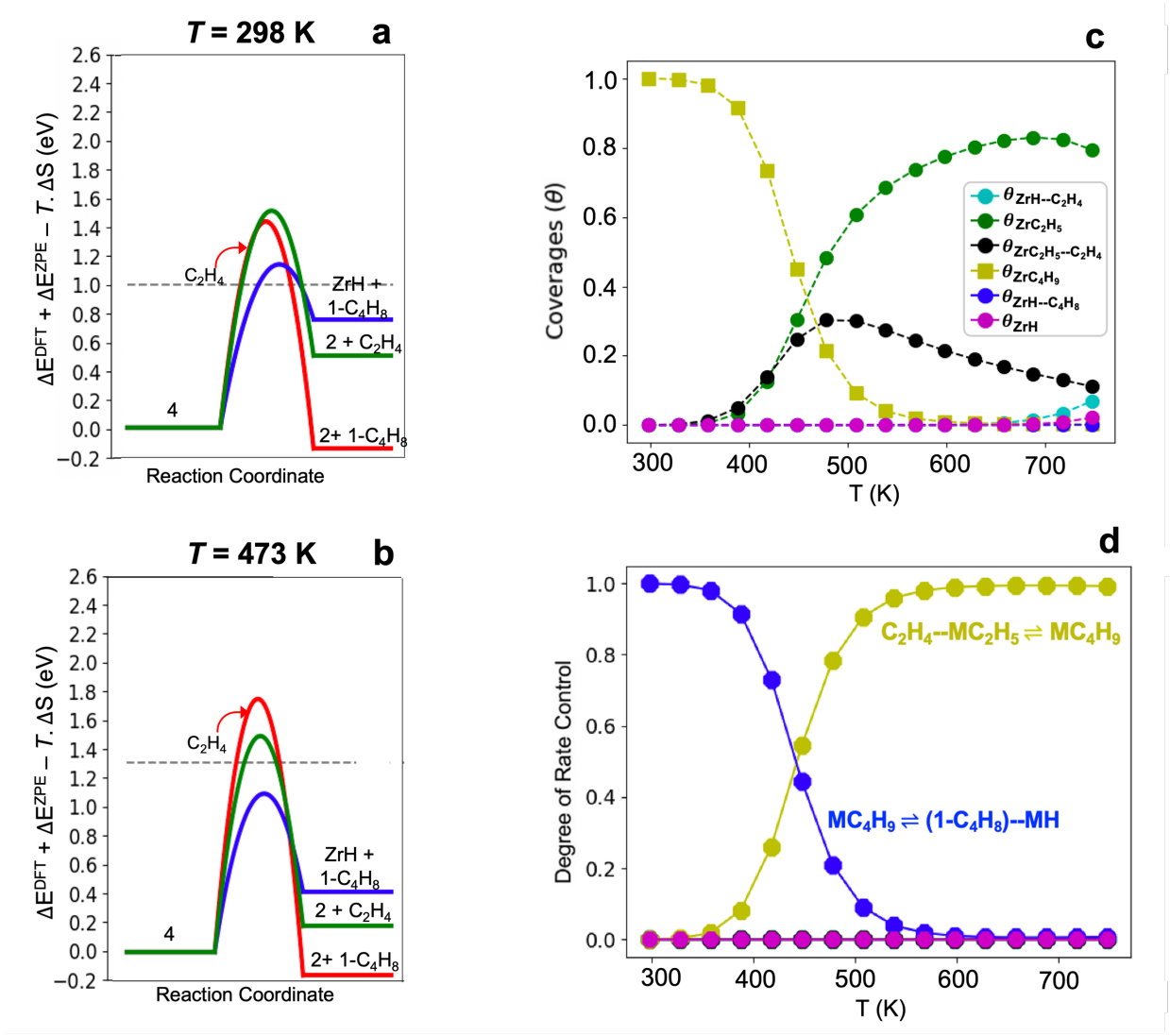

Fig. S18: (a,b) Termination vs oligomerization free energy surfaces at 3-3mr $(SiO)_3ZrH$ site at 298 and 473 K and 1 bar ethylene. Termination routes color coded as in Fig. 4: **(c)** Steady state coverages vs temperature at P_{C2H4} =17 bar **d)** Degree of rate control at P_{C2H4} =17 bar. Reactions color-coded as in Fig. S11.

Table S16: (top) Activation energies for chain growth via TS(2) and termination via TS(3a), bim-TS(3a), TS(3b), TS(3c) and TS(3d) for 3-3mr $(SiO)_3ZrH$ site at T = 0 K, 298 K and 473 K. (bottom) Consequences of various termination routes on computed $\overline{P_n}$ at low and high ethylene pressure (P_{C2H4}).

Reactions	$\Delta E^{\neq}$ (eV)	$\Delta G^{\neq,298K}$ (eV)		$\Delta G^{\neq,473K}$ (eV)	
C_2H_4 + MC_2H_5 → TS(2)	0.53	0.994		1.314	
MC_4H_9 → TS(3a)	1.172	1.172		1.172	
C_2H_4 + MC_4H_9 → bim-TS(3a)	1.01	1.474		1.794	
C_2H_4 + MC_4H_9 → TS(3c)	0.966	1.43		1.75	
MC_4H_9 → TS(3b)	1.492	1.492		1.492	
C_2H_4 + MC_4H_9 → TS(3d)	0.915	1.379		1.70	
		$\overline{P_n}$		$\overline{P_n}$	
$\overline{P_n}$ **Expressions**		P_{C2H4} = **0.27 bar**	P_{C2H4} = **17 bar**	P_{C2H4} = **0.27 bar**	P_{C2H4} = **17 bar**
$\overline{P_n} = 1+\frac{k_{CC}}{k_{term}}P_{C2H4}$ Where $k_{term} = k_{TS(3a)}$	-	277	1.74 x10^4	1.01	1.52
$\overline{P_n} = 1+\frac{k_{CC}}{k_{term}}P_{C2H4}$ where $k_{term} = k_{TS(3a)} + k_{TS(3b)} + P_{C2H4}.k_{TS(3c)} + P_{C2H4}k_{bim-TS(3a)} + P_{C2H4}k_{TS(3d)}$	-	277	1.73 x10^4	1.01	1.52

† $k_{TS(3a)}$, $k_{TS(3b)}$, $k_{TS(3c)}$, $k_{TS(3d)}$, $k_{bim-TS(3a)}$ are rate constant for different chain termination processes. k_{CC} is chain growth rate constant. $\Delta E^{\neq}$ is ZPE corrected DFT energy barrier and $\Delta G^{\neq}$ is free energy barriers at a given temperature

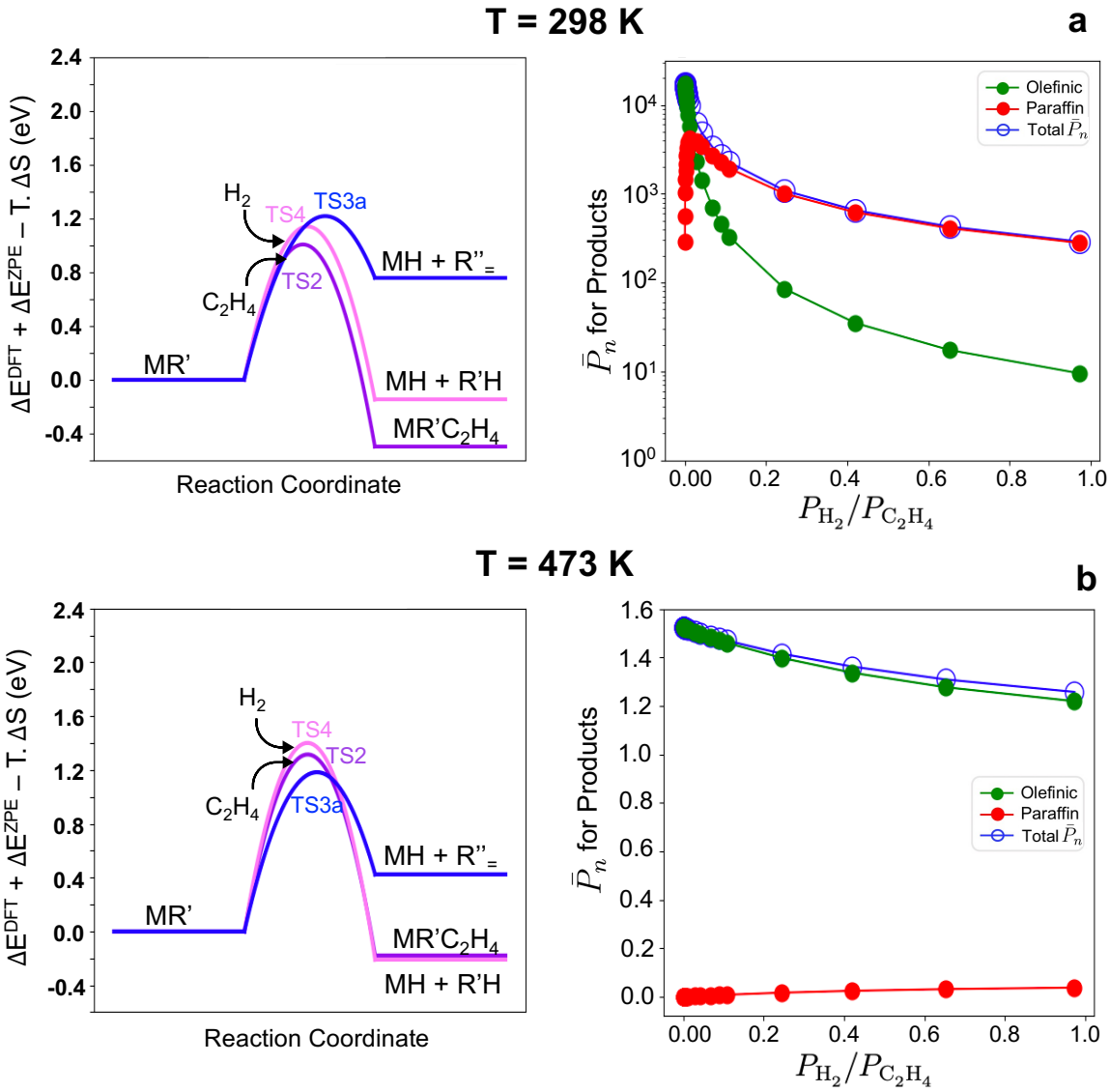

Fig. S19: Free energy profiles for the 3-3mr Zr-alkyl (MR') surface site along and corresponding $\overline{P_n}$ changes with P_{H2}/P_{C2H4} from 0 to 1 at **a)** T = 298 K **b)** T = 473 K for **1)** M-C insertion upon ethylene coordination via TS(2), **2)** hydrogenolysis upon hydrogen addition via TS(4), **3)** termination by β-H transfer to M via (TS3a) to olefin (R''=).

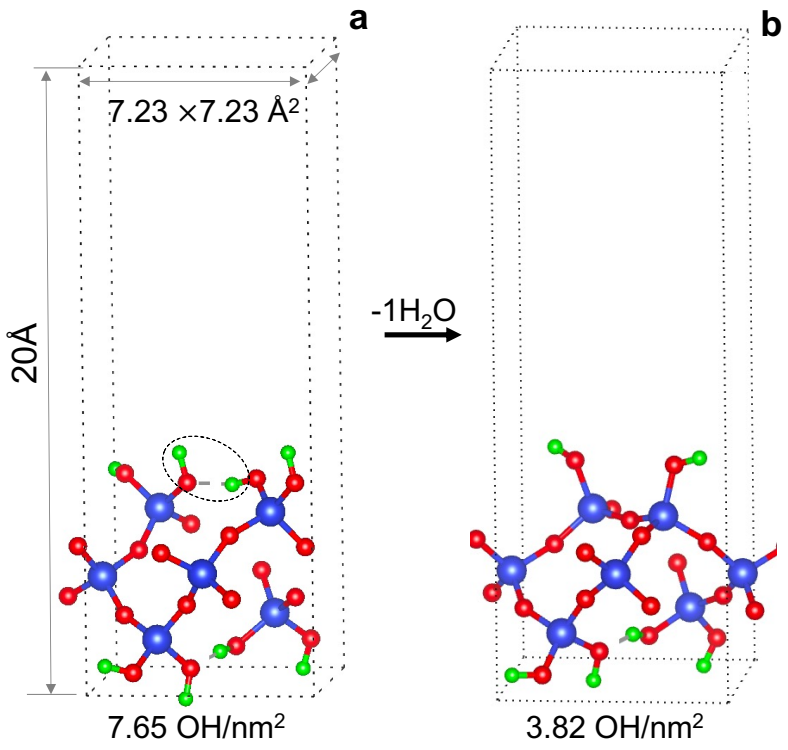

Fig. S20: a) (001) silica surface with geminal silanols and two Si-OHs that are condensed are circled **b)** Dehydroxylated (001) silica surface having the new Si-O-Si bond between the two silanols left on top.

Grafting and hydrogenolysis of $M(CH_3)_4$ to 1-3mr site

Grafting of $M(CH_3)_4$ on silanols of dehydroxylated (001) silica surface (Fig. S20b) is performed as per reaction (s1) to form $(\equiv SiO)_nM(CH_3)_{4-n}$ species on surface, where n=1, 2 and their further transformation to hydrides occurs as per reactions (s2). Thermodynamics of sequential grafted complexes of $Zr(CH_3)_4$ and their hydrogenation is shown in Fig. S21a, while Fig. S21b compares heats of grafting (ΔE_{rxn}^{DFT}) of $M(CH_3)_4$ on the (001) silica against $(\equiv SiO)_nZr(CH_3)_{4-n}$ on (111) silica. Grafting is exothermic for all species. Structural energies are in Table S17 and reaction energies in Table S18. Structures of $(\equiv SiO)_nM(CH_3)_{4-n}$, and $(\equiv SiO)_nM(H)_{4-n}$ are in Fig. S22 in the top row and bottom row, respectively.
A non-periodic trend is visible in hydrogenolysis energies on (001) facet (Table S18), alike that on silica (111) surface (Table S3).

Table S17: PBE computed energies E^{DFT} **(***without ZPE correction*) in eV for structures in grafting and hydrogenolysis process on dehydroxylated (001) silica shown in Fig. S20b

		E^{DFT} (eV)		
Species	**n**	**Ti**	**Zr**	**Hf**
$(\equiv SiO)M(CH_3)_3$	1	-250.038	-251.087	-252.992
$(\equiv SiO)_2M(CH_3)_2$	2	-227.693	-228.708	-230.717
$(\equiv SiO)M(H)_3$	1	-198.590	-200.019	-201.891
$(\equiv SiO)_2M(H)_2$	2	-193.448	-194.584	-196.561
Clean dehydroxylated (001) silica	-	-185.500		

Table S18: DFT computed heats of grafting $M(CH_3)_4$ on dehydroxylated silica (001) surface using energies (in eV) from Table S17

M	Grafting $M(CH_3)_4$ on silica (001) Calculated by reaction (s1)		Hydrogenolysis of grafted $(SiO)_nM(CH_3)_{4-n}$ Calculated by reaction (s2)	
	n=1	n=2	n=1	n=2
Ti	-2.03	-3.71	-0.37	-0.30
Zr	-2.16	-3.81	-0.74	-0.42
Hf	-2.20	-3.96	-0.71	-0.39

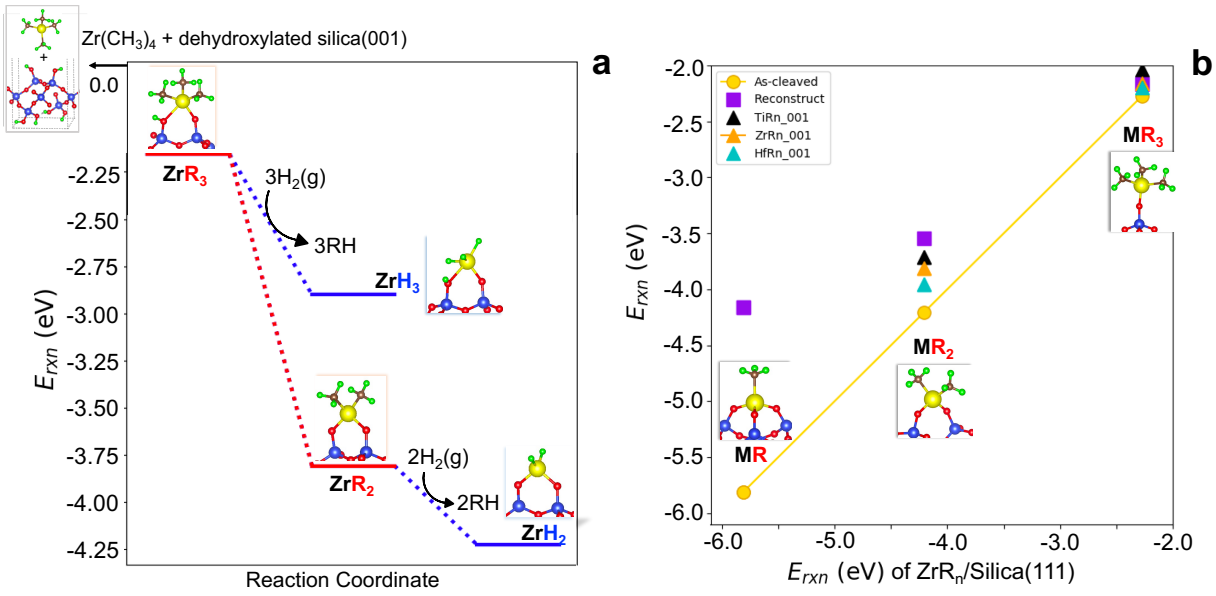

Fig. S21: a) Heats of formation of $(\equiv SiO)_nZr(CH_3)_{4-n}$ (R= CH_3) and hydrogenolysis to $(\equiv SiO)_nZr(H)_{4-n}$ [n=1,2] on dehydroxylated (001) silica **b)** Parity plot comparing heats of formation of $(\equiv SiO)_nM(CH_3)_{4-n}$ for Ti, Zr and Hf [n= 1, 2] on dehydroxylated silica (001) against $(\equiv SiO)_nZr(CH_3)_{4-n}$ on as-cleaved silica (111) [n = 1,2,3]. Energies of $(\equiv SiO)_nZr(CH_3)_{4-n}$ on reconstructed silica also shown.

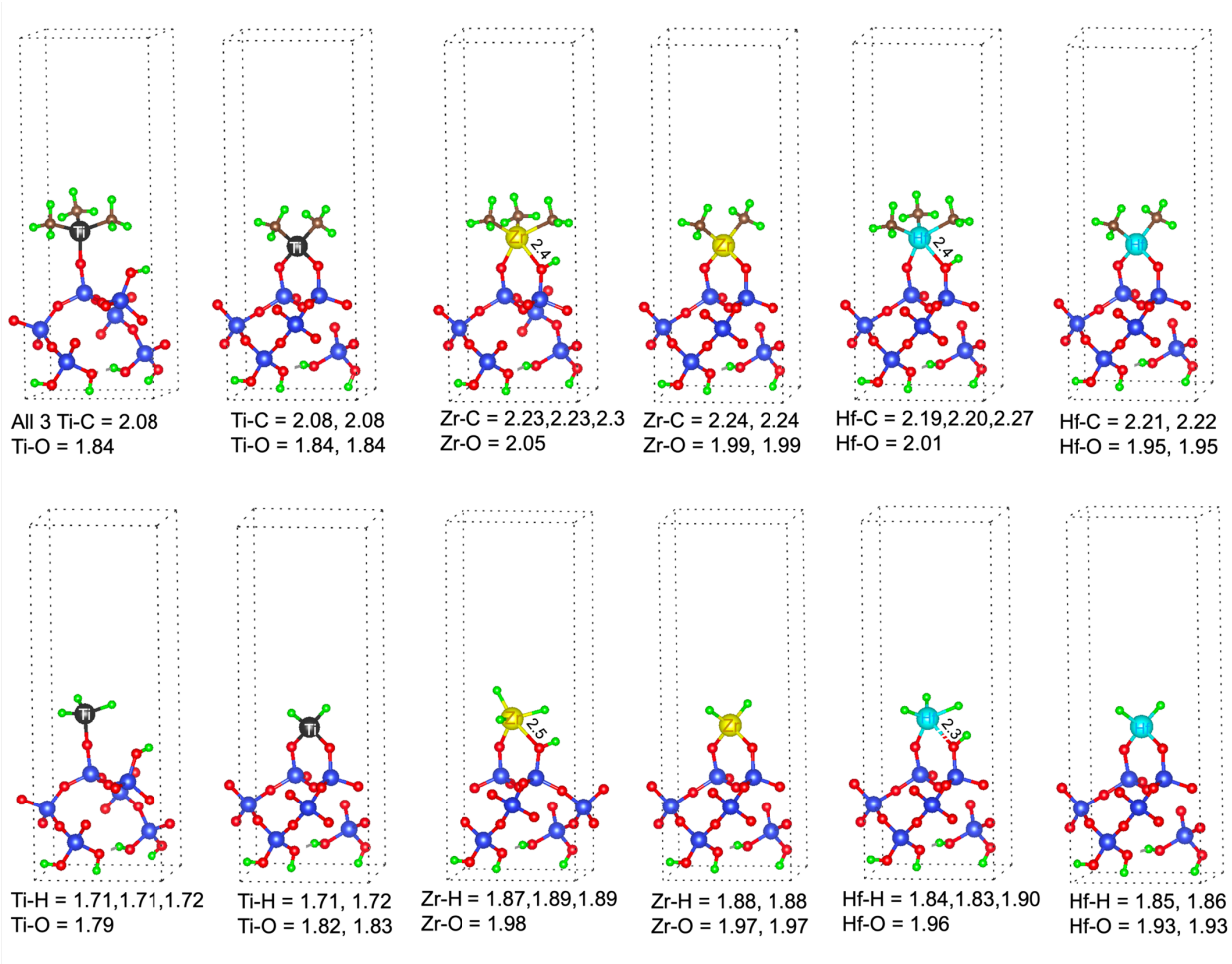

Fig. S22*:* Structures of $(\equiv SiO)_nM(CH_3)_{4-n}$ in top row and $(\equiv SiO)_nM(H)_{4-n}$ in bottom for Ti, Zr and Hf from left to right on dehydroxylated silica (001). H: green, C: brown, Si: blue, O: red. Distances in Å.

1-3mr oligomerization intermediates and reactions

Table S19: PBE computed energies **(E^{DFT},** *without ZPE correction***)** and zero-point energy (E^{ZPE}) correction in eV for different species on $(\equiv SiO)_2MH_2$ on silica (001)

	$(\equiv SiO)_2$**Ti**H_2		$(\equiv SiO)_2$**Zr**H_2		$(\equiv SiO)_2$**Hf**H_2	
	E^{DFT}	E^{ZPE}	E^{DFT}	E^{ZPE}	E^{DFT}	E^{ZPE}
$(SiO)_2MH_2$ (clean)	-193.438	0.387	-194.549	0.353	-196.528	0.357
C_2H_4--$(SiO)_2MH_2$	-225.732	1.812	-227.079	1.791	-228.991	1.800
$(SiO)_2MH(C_2H_5)$	-227.156	1.911	-228.210	1.876	-230.123	1.873
C_2H_4--$MH(C_2H_5)(SiO)_2$	-259.271	3.327	-260.495	3.285	-262.402	3.285
TS(1')	-259.186	3.340	-260.406	3.291	-262.249	3.293
$(SiO)_2M(C_2H_5)_2$	-260.548	3.418	-261.494	3.396	-263.443	3.387
C_2H_4--$M(C_2H_5)_2(SiO)_2$	-292.592	4.805	-293.527	4.829	-295.467	4.771
TS(2')	-291.916	4.916	-293.219	4.868	-295.031	4.860
$(SiO)_2M(C_2H_5)(C_4H_9)$	-293.743	4.949	-294.707	4.909	-296.656	4.914
TS(3'a)	-292.322	4.829	-293.547	4.788	-295.402	4.787
$(1\text{-}C_4H_8)$--$M(C_2H_5)(SiO)_2$	-292.448	4.836	-293.669	4.803	-295.550	4.798

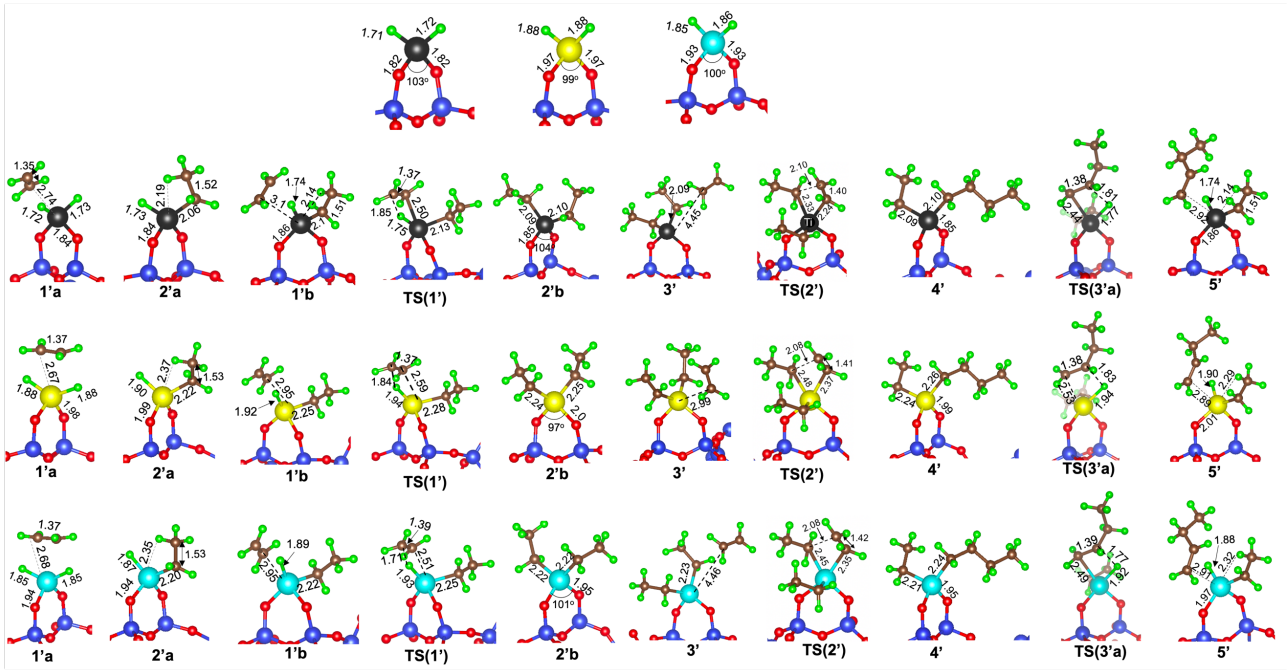

Fig. S23: Geometries of species along the catalytic cycle on $(\equiv SiO)_2MH_2$ site [M= Ti, Zr, Hf] on dehydroxylated (001) silica. Top row shows $(\equiv SiO)_2MH_2$ site, followed by species for $(\equiv SiO)_2$**Ti**H_2, then by $(\equiv SiO)_2$**Zr**H_2 and last row for $(\equiv SiO)_2$**Hf**H_2. Bond distances in Å. Angles in degrees (°). CONTCARs in Zenodo.[11]

Table S20: ZPE corrected heats of reactions (*dE*) in eV for ethylene dimerization on $(\equiv SiO)_2M(H)_2$. The barrier (*Ea*) is the energy differences between transition state and initial state at infinite separation. If a value is negative, we treat it as barrierless. For non-activated adsorption, the barriers are assumed to be 0

No.	Reactions	Ti		Zr		Hf	
		Ea	***dE***	***Ea***	***dE***	***Ea***	***dE***
1*	$C_2H_4 + MH_2 \rightarrow C_2H_4\text{--}M(H)_2$	0.0	-0.26	0.0	-0.48	0.0	-0.41
2	$C_2H_4\text{--}M(H)_2 \rightarrow MH(C_2H_5)$	0.0	-1.33	0.0	-1.05	0.0	-1.06
3*	$C_2H_4 + MH(C_2H_5) \rightarrow C_2H_4\text{--}MH(C_2H_5)$	0.0	-0.09	0.0	-0.27	0.0	-0.26
4	$C_2H_4\text{--}MH(C_2H_5) \rightarrow M(C_2H_5)_2$	0.13	-1.19	0.10	-0.89	0.16	-0.94
5*	$C_2H_4 + M(C_2H_5)_2 \rightarrow C_2H_4\text{--}M(C_2H_5)_2$	0.0	-0.05	0.0	0.01	0.0	-0.03
6	$C_2H_4\text{--}M(C_2H_5)_2 \rightarrow M(C_2H_5)(C_4H_9)$	0.79	-1.01	0.35	-1.10	0.52	-1.05
7	$M(C_2H_5)(C_4H_9) \rightarrow C_4H_8\text{--}MH(C_2H_5)$	1.30	1.18	1.04	0.93	1.13	0.99
8*	$C_4H_8\text{--}MH(C_2H_5) \rightarrow 1\text{-}C_4H_8 + MH(C_2H_5)$	0.0	0.07	0.0	0.24	0.0	0.21

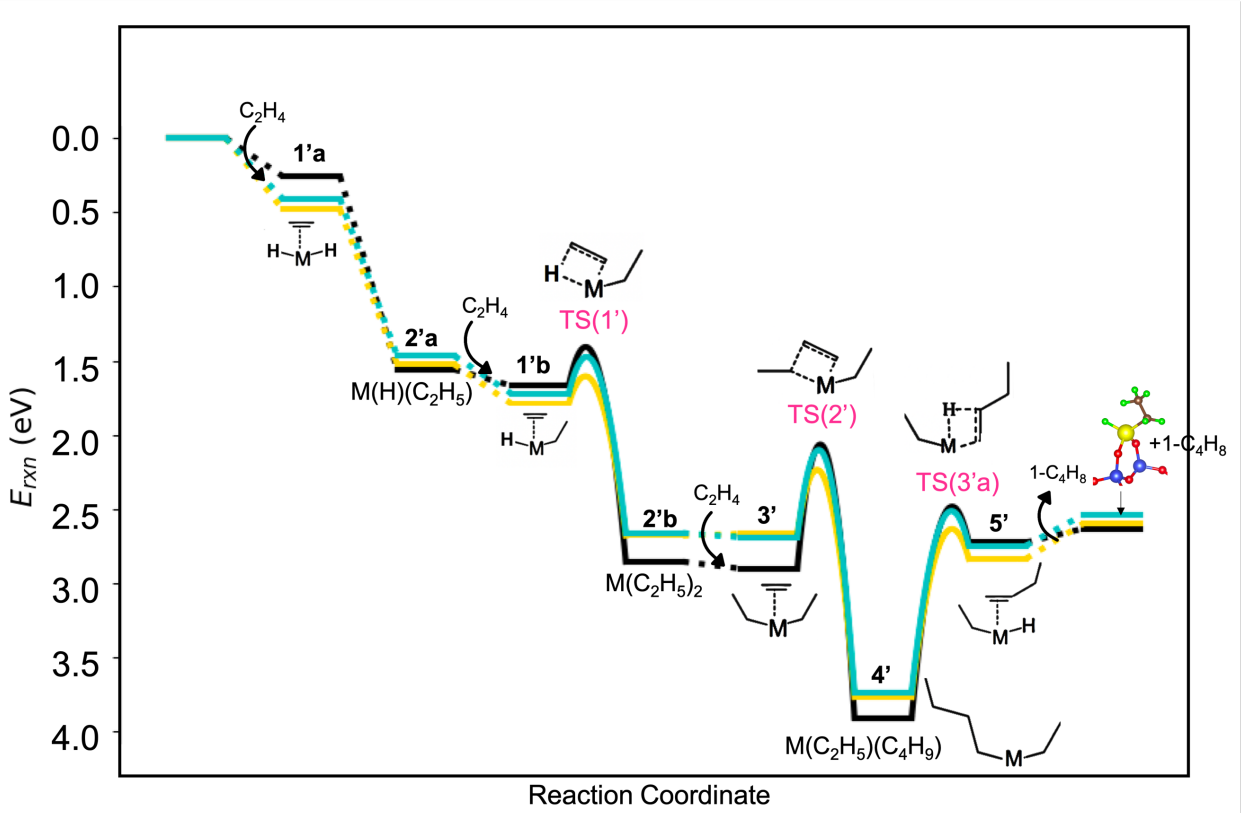

Fig. S24: PES for ethylene dimerization mechanism on (≡SiO)$_2$M(H)$_2$ grafted on dehydroxylated silica (001), M = **Ti (black)**, **Zr (yellow)** and **Hf (blue).** Energies are referenced to 1-3mr(≡SiO)$_2$M(H)$_2$ site and 3C_2H_4 gas molecules. Species numbers correspond to catalytic cycle shown in Fig. 11b.

The PES (Fig. S24) is referenced to the dihydride site, (≡SiO)$_2$MH$_2$ and ethylene molecules. Ethylene forms a stronger π-complex with (≡SiO)$_2$MH$_2$ than with (≡SiO)$_3$MH. The first ethylene insertion into M-H bond is exothermic and barrierless as no transition state is located when ethylene approaches the metal vertically downward rather than sideways (CI-NEB for Zr is similar to Hf in Fig. S26, Fig. S27 for Ti). It is further exogenic for ethylene to insert into the second M-H bond of (≡SiO)$_2$MH(C_2H_5) (**2'a**) and occurs via a four-centered transition state TS(1') (Fig. S23). TS(1') has a tiny barrier as compared to the next step of chain growth on (≡SiO)$_2$M(C_2H_5)$_2$ (**2'b**) to produce (≡SiO)$_2$M(C_2H_5)(C_4H_9) (**4'**) by M-C insertion of ethylene. The four-centered TS(2') (Fig. S23) shows ethylene conjoining M-ethyl to form the C-C bond approaches much closer to Ti than to Zr and Hf while the non-participating ethyl chain is aligned non-agostically. 1-butene is released from **4'** by endothermic ß-H transfer to M via TS(3'a) leaving behind (≡SiO)$_2$MH(C_2H_5), **2'a**. The order in energy barriers is $E_{a,term} > E_{a,C\text{-}C} > E_{a,M\text{-}H}$ for M(Et)H (Et = ethyl, C_2H_5) for M= Ti, Zr and Hf, same as that on 3-4mr (≡SiO)$_3$MH sites.

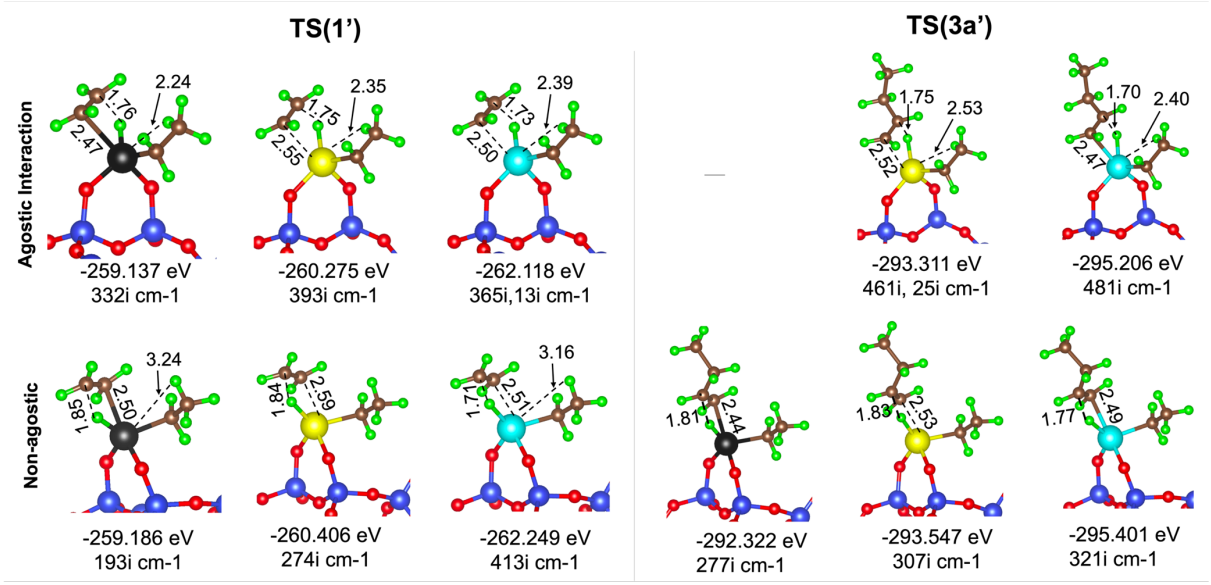

Fig. S25: TS(1') and TS(3'a) structures on left and right, respectively, with (top row) and without (bottom) agostic interaction of the side alkyl chain on $(\equiv SiO)_2MH_2$ site (M= Ti (black), Zr (yellow), Hf (blue)). E^{DFT} energies are lower for non-agostic structures.

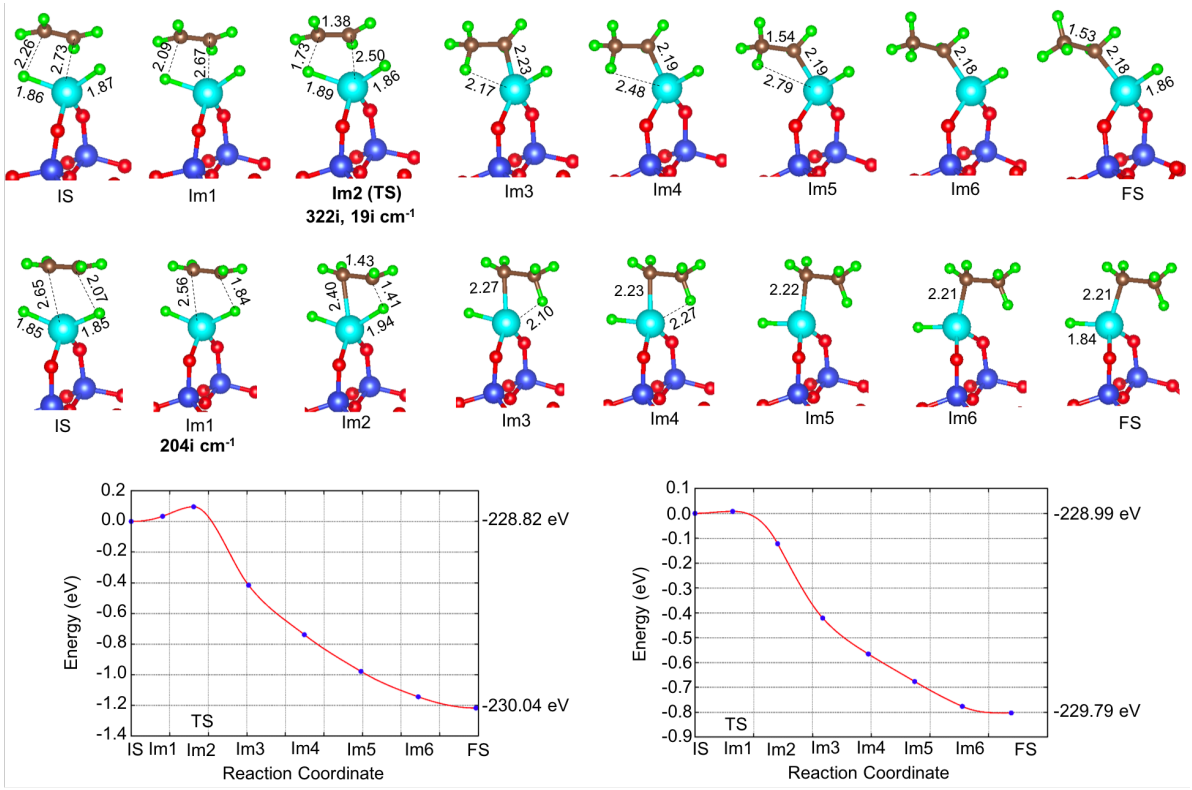

Fig. S26: CI-NEB trajectories for insertion of ethylene into Hf-H bond of $(\equiv SiO)_2HfH_2$. Similar trajectories found for this insertion into Zr-H bond of $(\equiv SiO)_2ZrH_2$. Top row shows ethylene coming sideways with energy graph on the left of bottom row. Middle row shows ethylene coming to M ion vertically downward and is zero barrier path from energy plot (right in bottom row). Distances in Å.

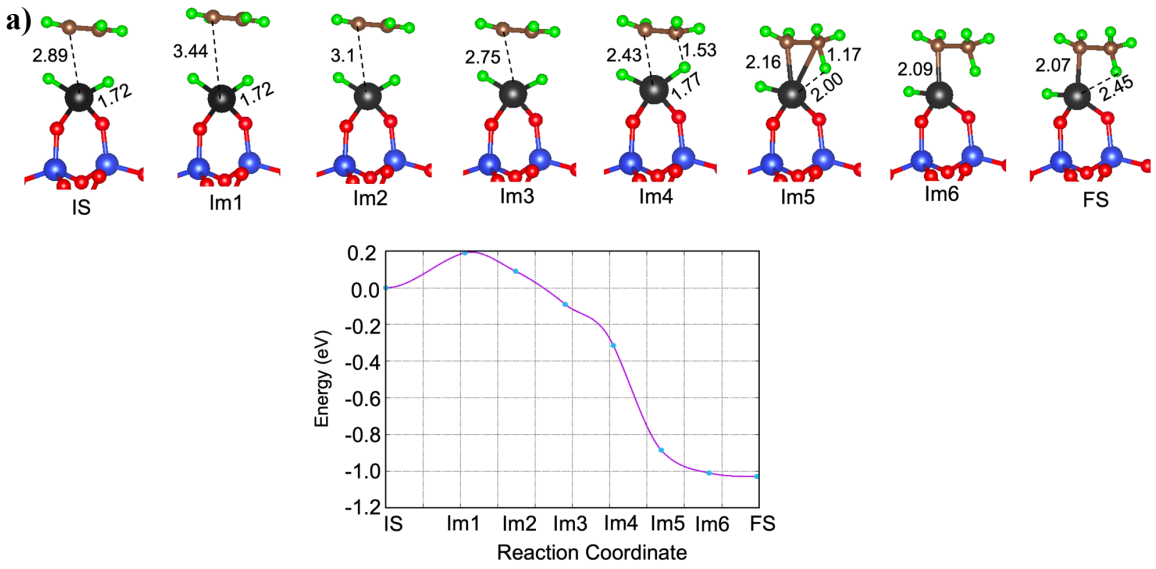
a)
2.89
1.72
IS
3.44
1.72
Im1
3.1
Im2
2.75
Im3
2.43
1.53
1.77
Im4
2.16
1.17
2.00
Im5
2.09
Im6
2.07
2.45
FS
Energy (eV)
0.2
0.0
-0.2
-0.4
-0.6
-0.8
-1.0
-1.2
IS Im1 Im2 Im3 Im4 Im5 Im6 FS
Reaction Coordinate

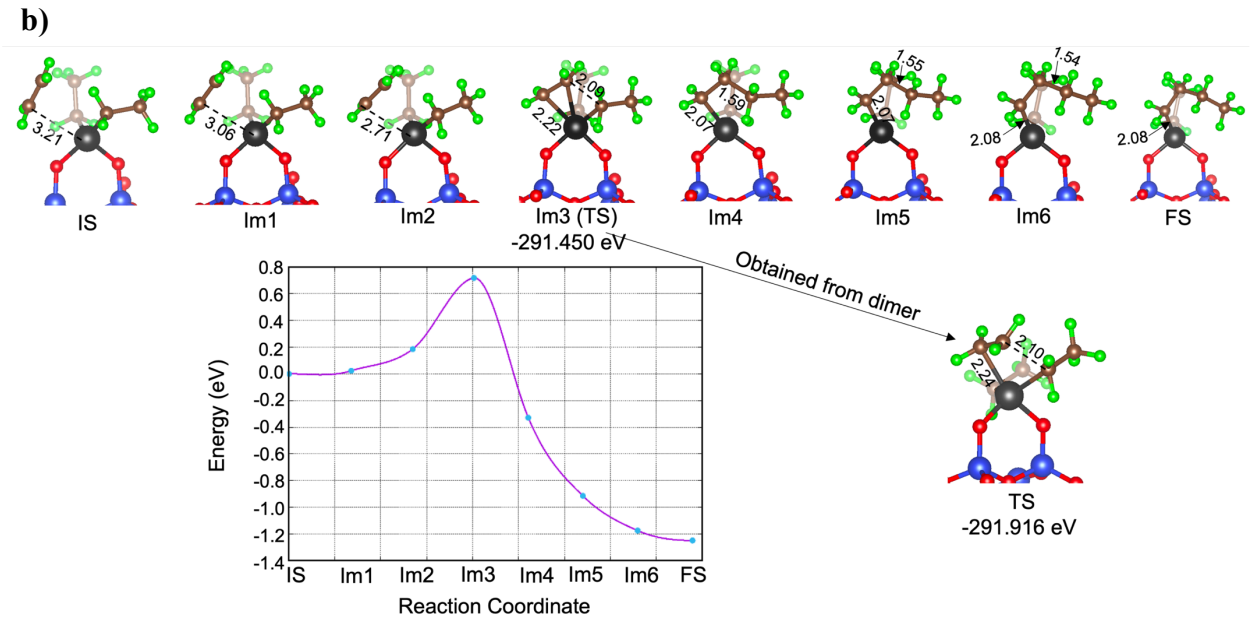
b)
3.21
IS
3.06
Im1
2.71
Im2
2.09
2.22
Im3 (TS)
-291.450 eV
1.59
2.07
Im4
1.55
2.07
Im5
1.54
2.08
Im6
2.08
FS
Obtained from dimer
2.10
2.24
TS
-291.916 eV
Energy (eV)
0.8
0.6
0.4
0.2
0.0
-0.2
-0.4
-0.6
-0.8
-1.0
-1.2
-1.4
IS Im1 Im2 Im3 Im4 Im5 Im6 FS
Reaction Coordinate

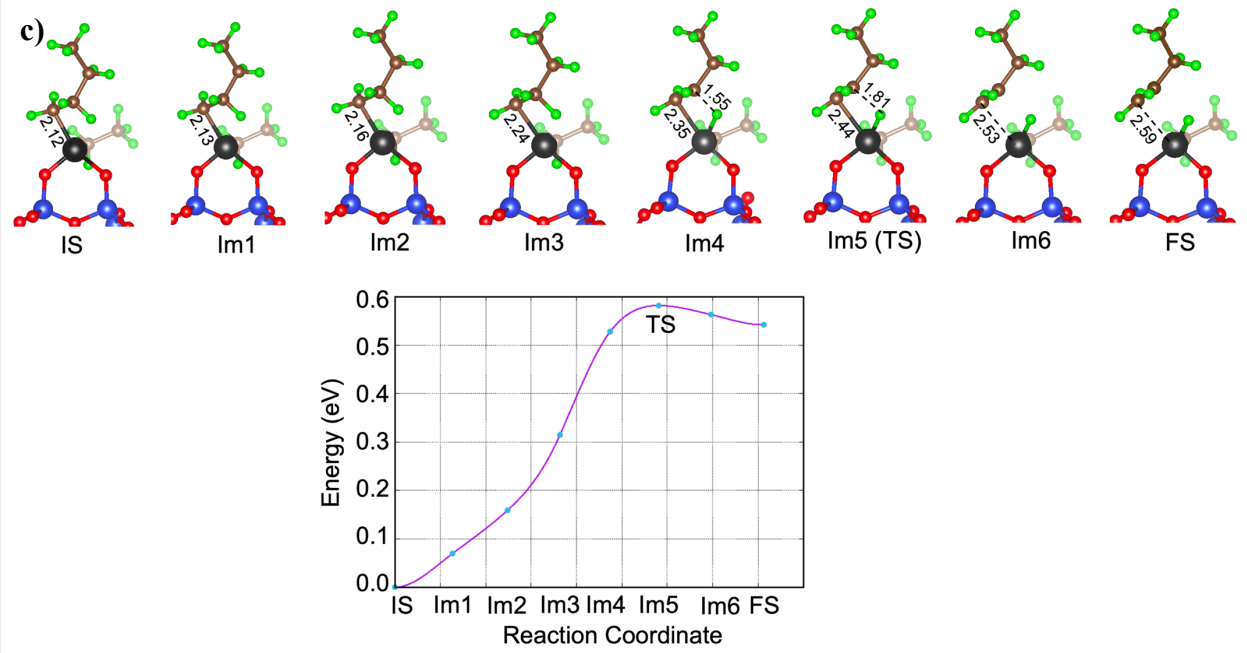

Fig. S27: CI-NEB images and energy graph for **a)** insertion of ethylene approaching vertically downward into Ti-H bond of $(\equiv SiO)_2TiH_2$ site. No transition state is located for this reaction step. **b)** ethylene insertion on one of the Ti-C bonds of $(\equiv SiO)_2Ti(Et)_2$ **c)** Termination by β-H transfer to M yielding 1-butene and $(\equiv SiO)_2Ti(H)(Et)$. Similar trajectories have been used to locate corresponding TSs on Zr and Hf sites. Distances in Å.

1-3mr microkinetic models

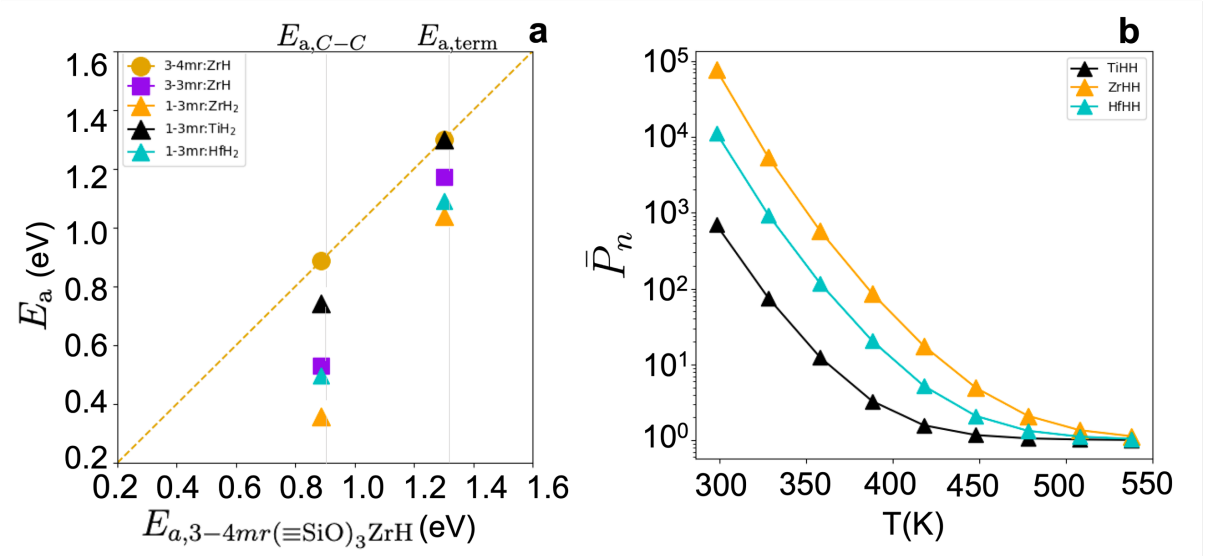

Fig. S28: a) Parity plot of activation energies of M-C insertion ($E_{a,C-C}$) and β-H termination to M ($E_{a,term}$) on 1-3mr $(\equiv SiO)_2MH_2$ (triangles) and 3-3mr $(\equiv SiO)_3MH$ (square) against those on 3-4mr $(\equiv SiO)_3ZrH$ (circle) sites **b)** $\overline{P_n}$ on log scale vs temperature at P_{C2H4}=17 bar for 1-3mr Ti (black), Zr (orange), Hf (blue) sites.

References

1) Wyckoff, R. W. G. Crystal Structures, 2nd ed., John Wiley & Sons, **1963**, vol. 1, chapter 4, 239.
2) Davidson, P. J.; Lappert, M. F.; Pearce, R., *Chem. Rev.*, **1976**, 76**,** 2, 219-242.
3) Larabi, C.; Merle, N.; Norsic, S.; Taoufik, M.; Baudouin, A.; Lucas, C.; Cazat, J. T.; Mallmann, A.; Basset, J. M., *Organometallics*, **2009**, 28, 5647–5655.
4) Thieuleux, C.; Quadrelli, E. A.; Basset, J. M.; Döbler, J.; Sauerb, J., *Chem. Commun.*, **2004**, 1729-1731.
5) Corker, J.; Lefebvre, F.; Lecuyer, C.; Dufaud, V.; Quignard, F.; Choplin, A.; Evans, J.; Basset, J.M., *J.-M. Science,* **1996,** 271 (5251), 966-969.
6) Tosin, G.; Santini, C. C.; Baudouin, A.; Mallman, A. d; Fiddy, S.; Dablemont, C.; and Basset, J.-M., *Organometallics,* **2007**, 26, 17, 4118-4127.
7) Lo, D. P.; Ray, W. H., *Ind. Eng. Chem. Res*., **2005**, 44, 5932-5949.
8) Campbell, C. T.; Sellers, J. R.V., *J. Am. Chem. Soc.,* **2012**, 134**,** 18109−18115.
9) Rosier, C.; Niccolai, G. P.; Basset, J.-M., *J. Am. Chem. Soc.* **1997,** *119,* 12408-12409.
10) Larsen, A. H. *et al*. *J. Phys.: Condens. Matter,* **2017**, 29, 273002.
11) Mehra, N.; Schneider, W. F. https://doi.org/10.5281/zenodo.11251373, 2024